Quaternary Science Reviews 369 (2025) 109599

Contents lists available at ScienceDirect

Quaternary Science Reviews

journal homepage: www.elsevier.com/locate/quascirev

Distal cryptotephra records in the Falkland Islands refine South American tephrochronology

Panayiotis Panaretos [a,b], Alistair J. Monteath [c,*], Zoë A. Thomas [d,**], Paul G. Albert [e], Britta J.L. Jensen [f], James Tamhane [a,b], Shaun Woudstra [f], Gwydion Jones [e], Rob Scaife [d], Michael J. Bentley [g]

[a] Earth and Sustainability Science Research Centre, School of Biological, Earth and Environmental Sciences, University of New South Wales, Sydney, Australia
[b] Chronos ^{14}Carbon-Cycle Facility, Mark Wainwright Analytical Centre, University of New South Wales, Australia
[c] British Antarctic Survey, Natural Environment Research Council, Cambridge, UK
[d] School of Geography and Environmental Science, University of Southampton, Southampton, UK
[e] Department of Geography, Swansea University, Singleton Park, Swansea, UK
[f] Department of Earth and Atmospheric Sciences, University of Alberta, Edmonton, Canada
[g] Department of Geography, Durham University, UK

ARTICLE INFO

Handling Editor Name: Biagio Giaccio

Keywords:
Tephrochronology
Falklands
Cryptotephra
Radiocarbon dating
South America
Southern ocean
Monte Burney
Reclus
Hudson
Chaitén
Aguilera

ABSTRACT

Cryptotephra (non-visible volcanic ash) deposits in the Falkland Islands (Islas Malvinas) provide a distal record of South American volcanism and ash dispersal into the South Atlantic Ocean. Here, we present three new cryptotephra records from peatlands in the archipelago and use these data to refine the age estimates of key regional tephra isochrons. Major-minor-trace element glass geochemistry and high-resolution radiocarbon chronologies were used to correlate cryptotephra deposits with known explosive eruptions at Reclus volcano (R1), Monte Burney and Hudson volcano (H2). We also identify cryptotephra deposits likely originating from Chaitén volcano, the Antillanca volcanic complex and two Mid Holocene eruptions of Aguilera volcano. Careful examination of major-minor element data from tephras linked with Monte Burney MB1 demonstrates discrepancies between medial and distal deposits preserved in Patagonia, Laguna Potrok Aike and the Falkland Islands. These suggest that two Early Holocene tephra deposits from Monte Burney may be widely distributed. Our integrated Bayesian age-depth model refines the median ages of Hudson H2 (4230–3775 calibrated years before present; cal yr BP), deposits from Monte Burney (as viewed from the Falkland Islands, 9540-9455 cal yr BP) and Reclus volcano R1 (14,800-14,060 cal yr BP). We also propose that the age of Aguilera A1 is older than previously suggested and dates to 4390-4150 cal yr BP. Our expanded geochemical dataset of volcanic glasses and new age constraints for these isochrons aid distal and near source tephra correlations and complement the current tephrochronological framework of the region.

1. Introduction

The tephrostratigraphy of the Falkland Islands provides a long-term record of explosive volcanism in the Southern Volcanic Zone (SVZ; 33–46 °S) and the Austral Andean Volcanic Zone (AVZ; 49–55°S), in southern South America (Fig. 1; Stern, 2004). Cryptotephra (non-visible volcanic ash) deposits erupted from volcanoes in these regions are found in high abundance throughout peat-stratigraphies in the archipelago and can be precisely dated using a combination of radiocarbon dating and Bayesian age-depth modelling (e.g., Thomas et al., 2019; Monteath et al., 2019; Panaretos et al., 2021). These data can help to refine volcanic hazard assessments (e.g., return intervals of major ash clouds) whilst also providing time-equivalent isochrons for palaeoenvironmental records in an important setting for understanding past changes in the Southern Hemisphere westerly wind belt (e.g., Turney et al., 2016; Thomas et al., 2018; Monteath et al., 2022; Tamhane et al., 2023).

Here, we present new cryptotephra records from three peat

* Corresponding author.
** Corresponding author.
E-mail addresses: alitea@bas.ac.uk (A.J. Monteath), z.thomas@soton.ac.uk (Z.A. Thomas).

https://doi.org/10.1016/j.quascirev.2025.109599
Received 6 June 2025; Received in revised form 19 August 2025; Accepted 23 August 2025
Available online 10 September 2025

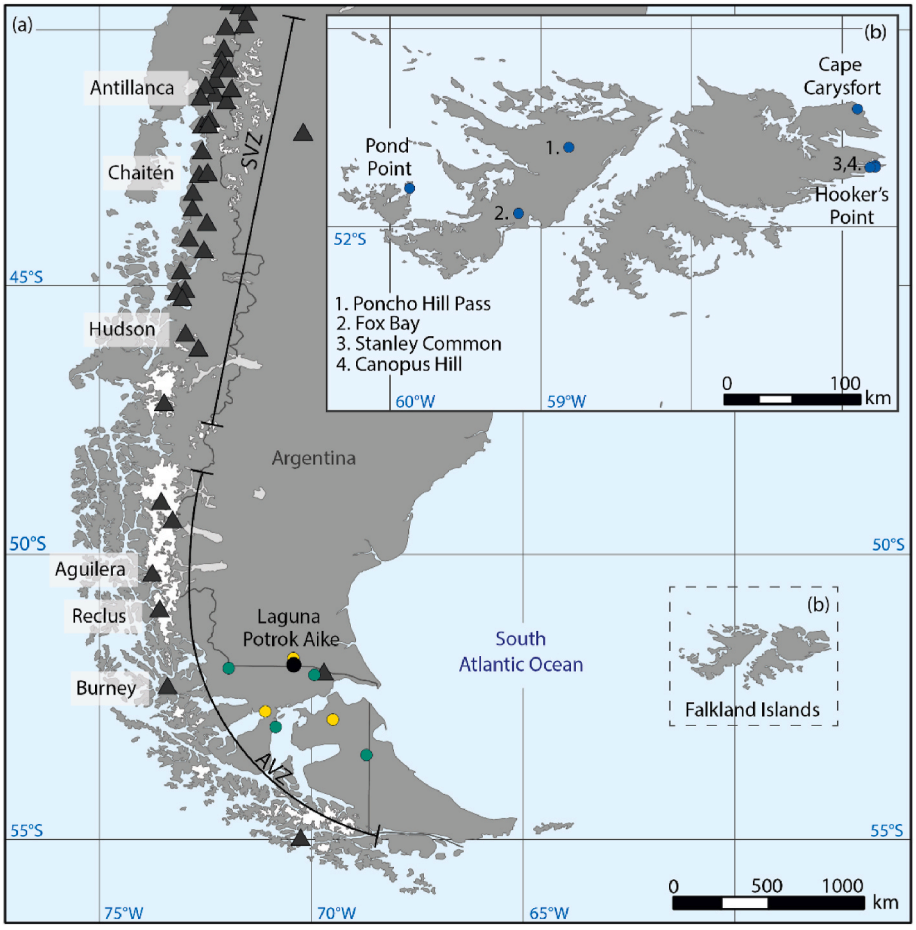

Fig. 1. Southern South America depicting (a) active (Holocene) volcanoes (Global Volcanism Program, 2025) from the Austral (AVZ) and Southern Volcanic Zones (SVZ) as defined by Stern (2004). Yellow (Del Carlo et al., 2018) and Green (Smith et al., 2019) dots indicate sampling locations of Monte Burney MB1 reference material. (b) Locations of cryptotephra records in the Falkland Islands. (Monteath et al. (2019); Panaretos et al., 2021; Hall et al., 2001).

sequences in the Falkland Islands, founded on high-resolution radiocarbon dating. We combine these data with existing records to produce an integrated Bayesian age-depth model and refine the ages of key volcanic isochrons from southern South America.

1.1. The tephrostratigraphy of the South Atlantic region

Numerous large explosive volcanic eruptions are known to have occurred in southern South America since the Last Glacial Maximum (Fig. 1), including at Monte Burney, Aguilera and Reclus volcanoes within the AVZ, and Hudson and Chaitén volcanoes in the SVZ (Fig. 1a; e.g., Stern, 2008; Fontijn et al., 2014). Tephra from these volcanic sources is preserved throughout southern South America in a variety of depositional sequences including marine, lake, peat-bogs, coastal aeolian deposits and stalagmites (Fontaine et al., 2021; Stern, 2008; Kilian et al., 2003; Weller et al., 2015; Fontijn et al., 2016; Zanchetta et al., 2021; Klaes et al., 2022). Recent work has demonstrated that tephra from the AVZ and SVZ can be dispersed well beyond the South American mainland. For example, ash from the recent eruptions of Hudson (1991 CE) and Puyehue-Córdon Caulle (2011 CE) has been identified in Antarctica (Koffman et al., 2017; Harlan et al., 2024). These findings highlight the potential for the investigation of Andean tephras in ultra-distal (>3000 km from source) settings, such as Antarctic ice cores, deposits on sub-Antarctic islands, and marine sediments in the Southern Ocean.

Cryptotephra studies in the Falkland Islands provide a distal tephra record of South America volcanism that can complement proximal and medial studies. A preliminary investigation by Hall et al. (2001) identified the presence of abundant microscopic ash and presented preliminary major-minor element data. Since then, three key marker horizons have been identified in the Falkland Islands. Monteath et al. (2019) correlated cryptotephra deposits at Hooker's Point, East Falkland, with Monte Burney (MB1; 10,640–8850 cal yr BP; Stern, 2008; Del Carlo et al., 2018; Smith et al., 2019) and Reclus volcanoes (R1; ca. 14, 730 cal yr BP; Stern et al., 2011). This study also highlighted some of the challenges with detrital and reworked ash which is common to many peat deposits in the Falkland Islands. More recently Panaretos et al. (2021) reported tephra from Hudson volcano (H2; 4200–3900 cal yr BP), including a full reference dataset of major-minor-trace-element geochemistry. These studies have improved our understanding on the dispersal of South American tephra, extending the known geographical extent of these isochrons to >1000 km from source. The three cryptotephra deposits identified in the Falkland Islands (R1, MB1 and H2) are the most distal identifications of these eruption deposits to date and are promising isochrons that could help assist chronological uncertainties in the South Atlantic and beyond.

2. Materials and methods

2.1. Study sites

The Falkland Islands are a small archipelago in the South Atlantic, 540 km east of southern South America. The islands lie at ~52°S, in the core of the Southern Hemisphere westerly wind belt, and experience high westerly airflow throughout the year (Upton and Shaw, 2002) that delivers dust, including tephra, mostly from Patagonia (Monteath et al.,

Table 1
Summary of cryptotephra deposits reported in this study. Age estimates come from independent age-depth models and are reported with median ages ± 2σ age ranges (Fig. 2).

Sample ID	Composite core depth (cm)	Median and 2σ age range (cal yr BP)	Source volcano	Notes
PP_89-90	89–90	3960 (4200-3770)	Hudson (H2)	Primary cryptotephra: ME/TE correlation to H2, supported by chronological constrains.
PP_176-177	176–177	9910 (10,150–9700)	Monte Burney	Primary cryptotephra: Correlates with CC_521–522 based on ME and TE glass data.
CC_142-143	142–143	2530 (2720-2370)	NA	Detrital, including Hudson tephra population
CC_199-200	199–200	3770 (3890-3650)	Hudson (H2)	Primary cryptotephra: ME and TE correlation to PP_89-90
CC_241-242	241–242	4280 (4390-4160)	Aguilera (AF1)	Good chemical match to A1 tephra. An older and less-widespread Aguilera eruption
CC_255-256	255–256	4360 (4460-4200)	Unclear	Less evolved than A1 tephra. Sollipulli correlation not supported by some ME oxides.
CC_278-279	278–279	4850 (5210-4480)	Chaitén	Good chemical match with the historical VCha-2008 and Cha-1, but not the Pumalin/Cha-2 tephras
CC_521-522	521–522	9540 (9700-9440)	Monte Burney[a]	Correlates with PP_176-177
HP05_3-4	3–4	−28 (180 to −60)	NA	Detrital - includes some H3 tephra & unique sub-population
HP05_25-26	25–26	380 (500-140)	NA	Detrital
HP05_69-70	69–70	1190 (1500-1070)	NA	Not analysed
HP05_107-108	107–108	2020 (2380-1770)	Antillanca	Detrital with sub-population that matches Playas Blancas Negras tephra.
HP05_212-213	212–213	3990 (4150-3760)	Hudson (H2)	Strong ME correlation to H2 (HP05_212–213 TE not determined).
HP05_224-225	224–228	4180 (4510-3990)	Aguilera (AF1)	Good chemical match to A1 tephra. Correlates with CC_241–242.
HP05_258-259	258–259	5090 (5280-4880)	Chaitén	Minor offset from CC_278–279 (likely analytical variation) but good chronological match. Matches chemically with the Cha-1 and Cha-2008 but not the Pumalin/Cha-2 tephra
HP05_289-290	289–290	5720 (6300-5480)	Aguilera	Chemical match to CC_241–242 and HP 30–35. Likely represents an older Aguilera eruption.
HP20_12-13	437–438	14,280 (14,800–14,060)	Reclus (R1)	Major-minor-trace element correlation with R1 tephra.

[a] Tephra deposits linked with Monte Burney are geochemically complex and require further investigation (see sect. 3.1.2). Abbreviations; ME (Major elements); TE (Trace elements).

2022; Tamhane et al., 2023). Blanket peatlands cover extensive areas of the Falklands Islands and began to form after ca. 16,500 cal yr BP as effective moisture levels increased following the Last Glacial Maximum (Wilson et al., 2002; Scaife et al., 2019).

2.1.1. Pond Point

Pond Point is located on Weddell Island (51.80662° S, 60.87150° W, Fig. 1b), the westernmost major island of the Falklands archipelago. A 2.79 m peat sequence was taken using a D section corer from blanket peat at Pond Point in March 2020. Tamhane et al. (2023) presented chronology and sediment geochemistry from the sequence that spans from ca. 10,050 cal yr BP to present, with a hiatus between 2000 cal yr BP to near present caused by peat cutting. Two intervals from the Pond Point record were targeted where suspected tephra deposits were identified based on spikes in inorganic content and X-ray fluorescence (XRF) data (Tamhane et al., 2023). In this paper we present shard point counts (1-cm resolution) and glass major-minor-trace element analyses for these core sections.

2.1.2. Cape Carysfort

Cape Carysfort is located (51.40742° S, 57.90282° W; Fig. 1b), on the northeast coast of East Falkland. A 6.00 m core was taken using D section corer in March 2020. Cape Carysfort is a large domed peatland amongst low and undulating terrain, and is likely ombrotrophic, with vegetation dominated by whitegrass (*Cortaderia egmontiana*). We targeted two sections of the core; 1.20–3.04 m (5500–2000 cal yr BP) and 5.04–5.44 m (11,500–9100 cal yr BP), which represent time-periods where known tephra deposits have previously been reported in the Falkland Islands (Panaretos et al., 2021; Monteath et al., 2019).

2.1.3. Hooker's point

Hooker's Point is a coastal outcrop situated in the East Falkland, 3.5 km east of Port Stanley (51.70101° S, 57.78329° W; Fig. 1b). The exposed section of peat lies behind a cobble beach and includes 5 m of peat, overlying clays. The profile has been sampled on three separate occasions; in 2005, 2016 and 2020. Chronology, palaeoecological analyses, tephrostratigraphy and dust provenance data has been published from the lower portion of the (16,500–6500 cal yr BP) 2005 sampling transect (HP05) by Scaife et al. (2019) and Monteath et al. (2019, 2022). Groff et al. (2020) report pollen data and geochemistry from the sequence retrieved in 2016, but refer to the site as Surf Bay. Here, we present new chronology and glass major-minor element data from the previously un-analysed, upper portion of the 2005 transect which spans ca. 6000–present (HP05). We also resampled the late Pleistocene portion of the sequence in 2020 to refine the age-model for the R1 tephra

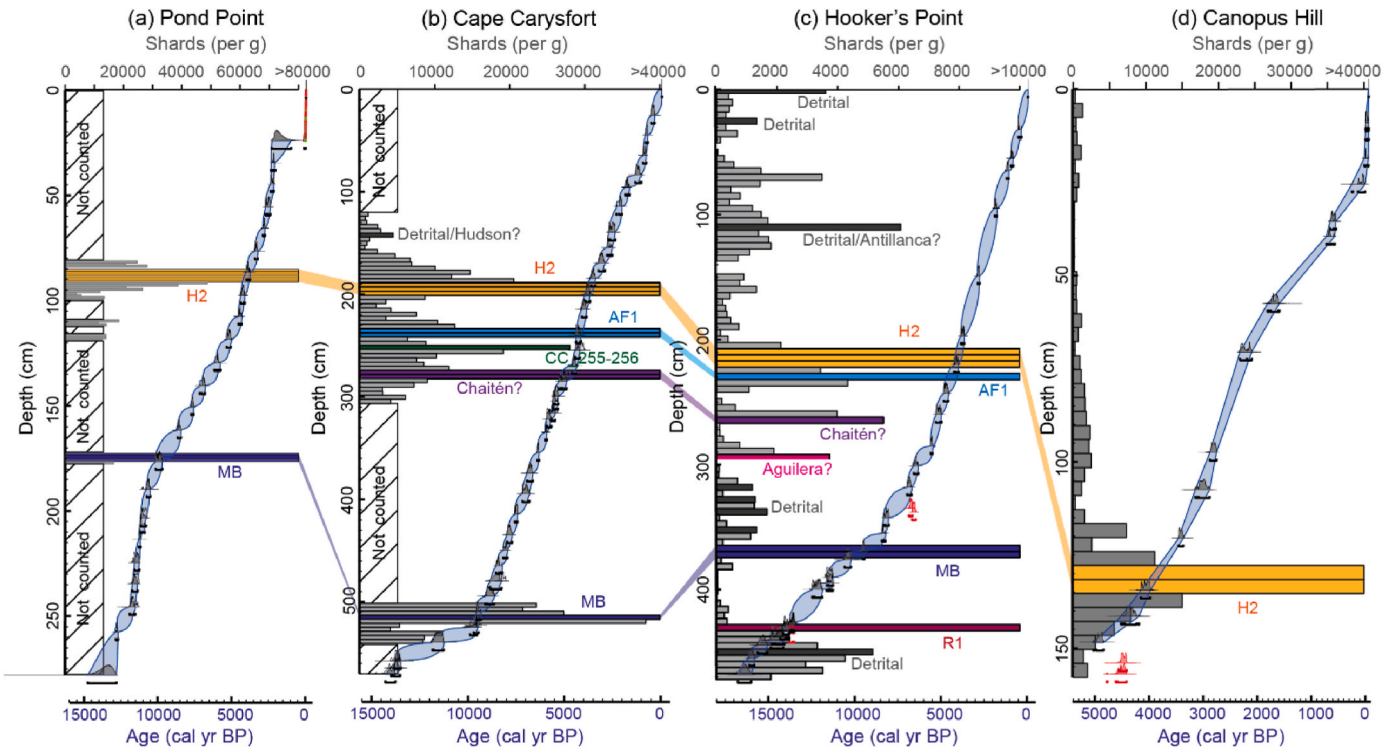

Fig. 2. Combined diagram of tephra concentrations and age-depth models for (a) Pond Point (Tamhane et al., 2023; this study), (b) Cape Carysfort (this study), (c) Hooker's Point 05 (Monteath et al., 2019; this study) and (d) Canopus Hill (Panaretos et al., 2021). Counts for 1-cm resolution samples can be found in the Supplementary Information (section 2.1).

(HP20). In all cases, the peat profile was sampled using a series of monolith tins that were pushed into overlapping, cleaned, cliff sections.

2.1.4. Canopus Hill

Canopus Hill (51.691° S, 57.785° W) is situated just outside Port Stanley on East Falkland. In 2011 a 1.60 m peat sequence was extracted with a D-section corer from blanket peat dominated by diddle dee (*Empetrum rubrum*) and whitegrass. Pollen and charcoal data are published in Turney et al. (2016), and a cryptotephra record identifying Hudson H2 using major-minor-trace element analysis was published in Panaretos et al. (2021).

2.2. Tephrostratigraphy

The methods used to quantify cryptotephra shards varied slightly between sites but are founded on standard protocols outlined in Pilcher and Hall (1992). Peat from Hooker's Point sequence HP05 was ashed at 550 °C for 2 h, sieved at 80 and 15 μm, and mounted for quantification under a high-power microscope. Peat from Hooker's Point sequence HP20, Cape Carysfort and Pond Point was ashed at 550 °C for 2 h and sieved at 90 and 25 μm. The HP20 and Pond Point samples required further processing and were subjected to density separation to extract glass from the host material (Blockley et al., 2005). Where high concentrations of tephra shards were identified, we processed additional samples at 1-cm intervals in the same manner to refine the stratigraphic position of cryptotephra deposits; identified by the highest concentration of tephra. The concentration of shards was determined as shard number per gram of dry sediment. Where shard concentrations were too high for counting (e.g., >10,000 per gram of dry sediment) in Hooker's Point sequence HP20, Cape Carysfort and Pond Point, counts were extrapolated based on the number of traverses across the slide (Supplementary Information, Section 1.1, Supplementary Data 2). In some cases, vertical reworking and high concentrations of tephra meant it was impossible to constrain the stratigraphic position of the isochron to less than 4–5 cm. In these cases, we used the mid-point of the shard-peak to define the position of the cryptotephra deposit.

2.3. Major-minor-trace element analysis of tephra deposits

Glass shards were extracted for electron probe microanalysis (EPMA) and laser ablation inductively-coupled plasma mass spectrometry (LA-ICP-MS) using density separation (Blockley et al., 2005), with the exception of shards from HP05 which were extracted using acid digestion (Dugmore et al., 1995). In all cases, shards were mounted in epoxy resin, sectioned and carbon coated prior to analysis.

2.3.1. Electron probe microanalysis (EPMA)

Major-minor elements were analysed using EPMA, with wavelength dispersive spectrometry, at the University of Alberta, the University of Oxford and the University of Edinburgh. The major-minor element compositions of glass shards are presented as normalised weight percent (wt %) oxides in comparative diagrams. All secondary standards analysed alongside the unknown cryptotephra samples, using the respective analytical setups described below, are provided in Supplementary Dataset 1.

The chemical composition of volcanic glass for the HP05 record was analysed using a JEOL 8900 Superprobe at the University of Alberta. A suite of 10 elements (Si, Ti, Al, Fe, Mn, Mg, Ca, Na, K, Cl) were measured using a 5 μm beam diameter with a 15 keV accelerating voltage, and 6 nA beam current, with time-dependent intensity corrections applied to Na to compensate for the narrow beam (<10 μm) diameter (e.g., Donovan et al., 2015; Jensen et al., 2021). In addition, we ran two

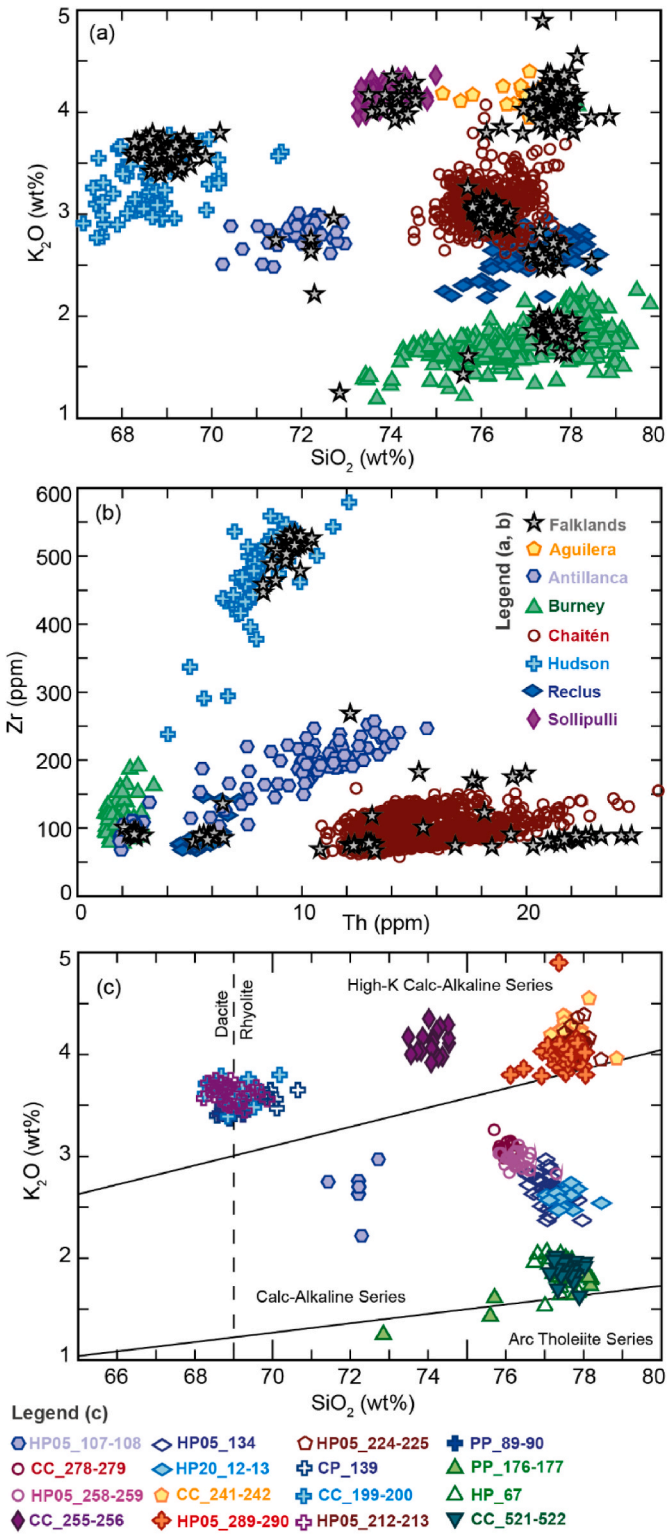

Fig. 3. (a) Major (EMPA) and (b) trace element (LA-ICP-MS) data from the Falkland Island cryptotephra deposits plotted against data from the South American BOOM database (Fontaine et al., 2023; references therein). Additional comparative data are from Panaretos et al. (2021) and Monteath et al. (2019). Note that LA-ICP-MS data is not available for all South American volcanoes or cryptotephra deposits from HP05. (c) Major element data from the Falkland Island cryptotephra deposits plotted following K_2O v SiO_2 nomenclature after Peccerillo and Taylor (1976).

natural glass secondary standards of known compositions alongside the volcanic glass samples to check for instrumental drift and analytical precision: i) Lipari rhyolitic obsidian ID3506 and ii) Old Crow tephra (Kuehn et al., 2011).

The major-minor element composition of volcanic glass from Pond Point and HP20 (the late Pleistocene section of Hooker's Point) was determined using a wavelength-dispersive JEOL JXA-8200 electron microprobe, equipped with five wavelength-dispersive spectrometers, at the School of Archaeology, University of Oxford. A beam accelerating voltage of 15 keV was used with a 6 nA current and a defocused beam diameter of 10 μm. The instrument was calibrated with a suite of appropriate mineral standards; peak count times were 30 s (s) for all elements except Mg (50s), Mn (50s), Na (12s), Cl (50s), and P (50s). Reference glasses from the Max Planck institute (MPI-DING suite; Jochum et al., 2006) bracketing the possible chemistries were analysed alongside the unknown tephra. These included felsic [ATHO-G (rhyolite)], through intermediate [StHs6/80-G (andesite)] to mafic [GOR132-G (komatiite)] glasses. Accuracies of analyses on these MPI-DING glasses were typically <5 % for concentrations >0.2 wt%.

Major element glass compositions of the Cape Carysfort cryptotephra samples were measured using a Cameca SX100 electron microprobe (EMPA), with five wavelength dispersive spectrometers, at the Tephra Analytical Unit, University of Edinburgh. A suite of 11 elements (Si, Ti, Al, Fe, Mn, Mg, Ca, Na, K, P, Cl) were measured using a 5 μm beam diameter with a 15 KV accelerating voltage and a 2 nA current for high abundance elements (Si, Al, Fe, K, Ca, Na, Mg), while 80 nA was used for lower abundance elements (Ti, Mn, Cl, P), following Hayward (2012). Pure metals, synthetic oxides and silicate standards were used when calibrating the instrument. The secondary standards of Lipari (Cannetto Lami Lava) and BCR2g were analysed at regular intervals to monitor for instrumental drift across the analytical session, and to evaluate the precision and accuracy of analysed samples.

2.3.2. Laser ablation inductively-coupled plasma mass spectrometry (LA-ICP-MS)

Trace element analysis of volcanic glass from the Pond Point, Cape Carysfort and Hooker's Point (HP20 only) was performed using an Agilent 8900 triple quadrupole ICP-MS (ICP QQQ) coupled to a Resonetics 193 nm ArF excimer laser-ablation (LA-ICPMS) in the Department of Earth Sciences, Royal Holloway, University of London. The full analytical procedures used are reported in Tomlinson et al. (2010). A crater spot size of 25 or 20 μm was used depending on shard sizes. The repetition rate was 5 Hz, with a count time of 40 s on the sample, and 40 s on the gas blank to allow for the subtraction of the background signal. Blocks of eight or nine glass shards and one MPI-DING reference glass (Jochum et al., 2006) were bracketed by the NIST612 glass calibration standard (GeoREM 11/2006) to monitor the accuracy of the data. The internal standard applied was ^{29}Si, which was determined using the electron microprobe. LA-ICP-MS data reduction was performed in Microsoft Excel. Accuracies of analyses of MPI-DING glass standards ATHO-G and StHs6/80-G were typically ≤5 % for most elements. Full glass datasets for the Pond Point and Cape Carysfort cryptotephra deposits are provided in Supplementary Dataset 1, along with analyses of the MPI-DING glasses.

2.4. Radiocarbon dating and tephra Bayesian age modelling

2.4.1. Radiocarbon dating

Seventy-two new AMS-derived radiocarbon dates were generated from peat deposits at the CHRONOS ^{14}Carbon-Cycle Facility, University of New South Wales, Australia (Table S6). Samples were dispersed in Milli-Q water then washed through a 250 μm sieve to remove root and rootlet material, and identify macrofossils (Thomas et al., 2019). In total

18 plant macrofossils were extracted. Where no macrofossils could be identified, sieved samples (<250 μm fraction) were then prepared for dating using an acid-base-acid treatment, following Turney et al. (2021).

2.4.2. Bayesian age depth models

We developed a Bayesian age-depth model for each site using OxCal v.4.4.4 (Bronk Ramsey, 2009a) and the SHCal20 and Bomb21SH1 Southern Hemisphere radiocarbon calibration curves (Hogg et al., 2020; Hua et al., 2021). For the Hooker's Point site, chronological data from the two peat sequences (HP05 and HP20) were merged into a single age-depth model based on loss on ignition data, the position of the R1 cryptotephra deposit and distance from the clay base (Fig. S15). For each site, radiocarbon dates were placed within a P_Sequence depositional model with a variable k parameter to independently determine the optimal variability in sedimentation rate (Bronk Ramsey, 2008; Bronk Ramsey and Lee, 2013). A General_Outlier model was applied with a 5 % prior probability of any individual date being a statistical outlier (Bronk Ramsey, 2009b). Modelled ages are reported here as median ages or two-sigma uncertainties (95.4 % of the probability distribution). Importantly, Bayesian age modelling of sequential sediment sequences exploits the stratigraphic ordering of the radiocarbon ages. This 'prior' information can reduce the uncertainties associated with calibrating radiocarbon ages and help to constrain the ages of cryptotephra deposits.

To more accurately model the ages of cryptotephra deposits that are common to multiple peat sequences in the Falkland Islands we combined the age models for each site using the ' = ' operator (Bronk Ramsey, 2009a). Four eruptions which were identified across multiple sites were used as tie-points. This included the H2 and AF1 deposits (see section 3.2), as well as deposits originating from Chaitén and Monte Burney (MB). The resulting ages for these cryptotephra deposits represent robust age estimates that can be applied to future sediment records where these isochrons are found.

3. Results and discussion

3.1. Tephrostratigraphy and chronology

We identified 13 primary cryptotephra deposits across the three new records presented in thisstudy, 11 of which can be linked with volcanic sources in southern South America (Table 1 and Figs. 2–3). Comparison between major-minor elements from cryptotephra deposits in the Falkland Islands and the BOOM database (Fontaine et al., 2023) indicates that volcanic glass from Monte Burney, Aguilera, Sollipulli, Hudson, Chaitén and Reclus volcanoes may be present in the Falkland Islands and these potential correlations are investigated more closely in the following discussion (Fig. 3). A further five cryptotephra deposits in the Falkland Islands are formed of weathered glass with mixed major-minor element compositions and are likely to represent the deposition of reworked detrital glass from Patagonia (Monteath et al., 2019). In some cases, major-minor element glass populations may represent primary airfall, however, they are difficult into interpret amongst re-worked material. Full datasets from these detrital deposits are available in Supplementary information but they are not discussed further.

3.1.1. Reclus volcano

Cryptotephra deposit HP20_12–13 in Hooker's Point, is formed of abundant (~50,000 shards per gram), clear, cuspate, platy shards, with high SiO_2 (avg. 77.50 wt%) and intermediate K_2O (avg. 2.60 wt%) values relative to other cryptotephra deposits in the Falkland Islands

Table 2
Mean and standard deviation glass major-minor element geochemistry for Falkland Islands cryptotephra deposits normalised to 100 %.

Sample	n	SiO_2	TiO_2	$Al2O_3$	FeO_T	MnO	MgO	CaO	Na_2O	K_2O	P_2O_5	Cl	H_2Odiff
Hudson													
PP_89-90	16	68.74	0.72	15.65	2.98	0.11	0.64	1.65	5.73	3.47	0.16	0.15	1.12
		0.99	0.13	0.14	0.40	0.02	0.18	0.26	0.13	0.16	0.09	0.02	0.81
HP05_212-213	23	68.92	0.69	15.67	2.91	0.10	0.62	1.54	5.81	3.62		0.17	0.97
		0.42	0.07	0.13	0.15	0.03	0.05	0.10	0.24	0.09		0.02	0.81
CC_199-200	23	69.00	0.68	15.19	2.85	0.11	0.64	1.60	5.98	3.62	0.12	0.20	0.11
		0.44	0.03	0.17	0.17	0.01	0.04	0.13	0.27	0.11	0.01	0.01	0.85
Aguilera													
CC_241-242	28	77.64	0.13	12.25	0.90	0.02	0.16	1.02	3.45	4.20	0.02	0.20	1.46
		0.23	0.00	0.17	0.07	0.01	0.01	0.04	0.17	0.12	0.00	0.03	1.60
HP05_224-225	27	77.83	0.15	12.43	0.90	0.02	0.15	0.98	3.32	4.08		0.18	3.20
		0.24	0.03	0.14	0.05	0.02	0.03	0.07	0.22	0.13		0.04	1.57
HP05_289-290	25	77.46	0.17	12.72	0.96	0.02	0.16	1.03	3.34	4.00		0.18	4.95
		0.46	0.03	0.34	0.08	0.02	0.02	0.06	0.28	0.21		0.05	1.84
Chaitén													
HP05_258-259	28	76.31	0.11	13.97	1.22	0.06	0.24	1.25	3.78	2.96		0.12	6.28
		0.29	0.03	0.20	0.05	0.02	0.02	0.03	0.17	0.07		0.04	2.33
CC_278-279	20	76.00	0.10	13.61	1.20	0.06	0.24	1.29	4.24	3.07	0.06	0.13	4.51
		0.18	0.00	0.21	0.09	0.01	0.00	0.03	0.15	0.07	0.00	0.05	1.86
Monte Burney													
CC_521-522	28	77.58	0.15	12.69	1.08	0.04	0.26	1.24	4.80	1.89	0.04	0.23	2.34
		0.24	0.01	0.18	0.07	0.00	0.01	0.09	0.13	0.09	0.00	0.02	1.60
PP_176-177	19	77.58	0.16	12.90	1.09	0.04	0.26	1.27	4.63	1.82	0.05	0.18	3.49
		0.54	0.05	0.19	0.15	0.02	0.06	0.24	0.13	0.12	0.03	0.01	1.42
Reclus													
HP20_12-13	18	77.50	0.11	12.95	1.16	0.03	0.20	1.46	3.78	2.60	0.03	0.18	3.61
		0.32	0.03	0.08	0.07	0.02	0.03	0.09	0.19	0.08	0.02	0.02	1.18
Antillanca													
HP05_107–108[a]	5	72.18	0.36	15.10	1.86	0.07	0.54	2.03	5.05	2.67		0.19	2.00
		0.42	0.04	0.18	0.04	0.03	0.05	0.07	0.39	0.25		0.03	1.03
Unknown													
CC_255-256	21	74.10	0.24	14.00	1.06	0.08	0.25	0.86	5.07	4.11	0.04	0.19	3.98
		0.29	0.01	0.28	0.08	0.01	0.01	0.05	0.20	0.13	0.00	0.03	2.09

[a] Indicates a sub-population of shards within a cryptotephra deposit. Note that the link with Antillanca requires further testing.

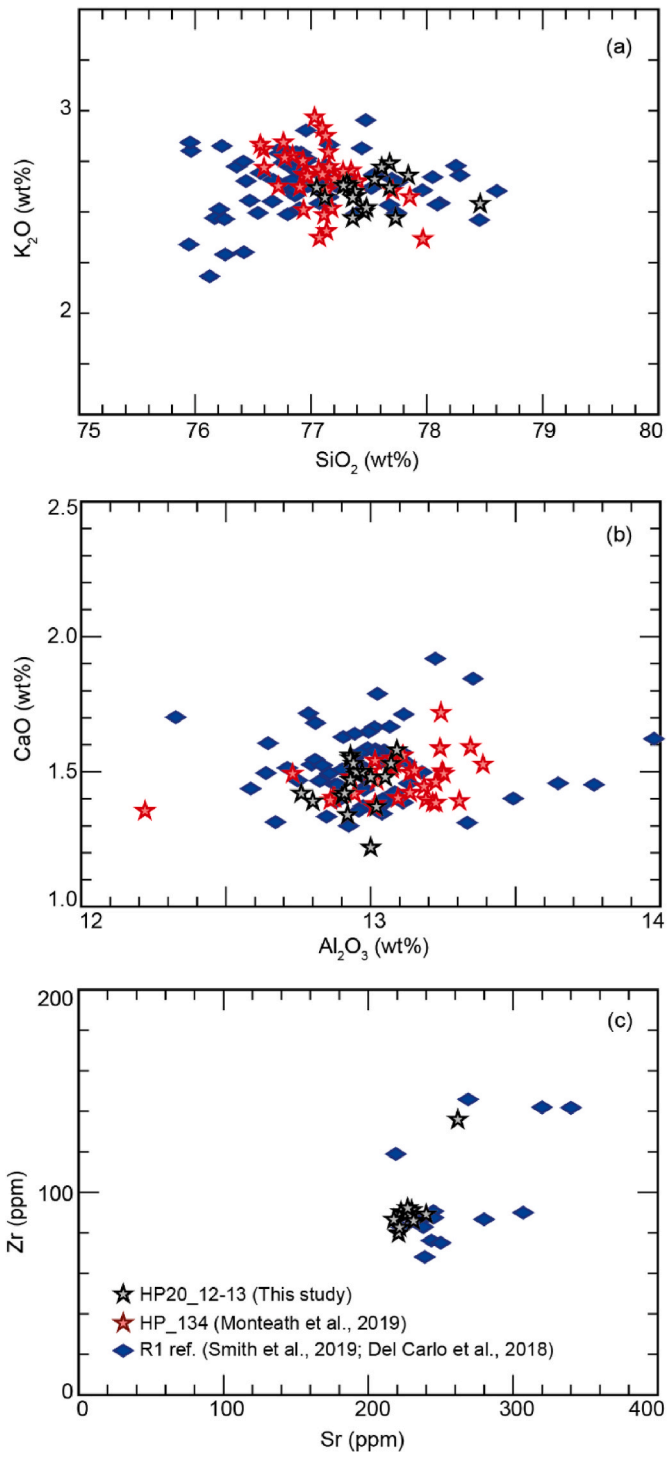

Fig. 4. Major and trace element biplots comparing volcanic glass data from the Falkland Islands cryptotephra deposits with medial deposits attributed to Reclus R1.

(Fig. 3, Table 2). The 2σ age range of HP20_12–13 is 14,800–14,060 cal yr BP. Major-minor elements from HP20_12–13 are indistinguishable from the Reclus Volcano R1 tephra (Del Carlo et al., 2018; Smith et al., 2019, Fig. 4). Trace elements are closely related although some minor offsets are evident (e.g., Rb 11.9 ppm, Nb 2.3 ppm, Ba 128.2 ppm; Del Carlo et al., 2018). These offsets are likely to represent differing instrumental conditions, however, and the Falklands Island cryptotephra deposit can be correlated with R1 tephra. The R1 tephra was deposited to the southeast of Reclus Volcano, towards the Falkland Islands, during one of the largest (Volcanic explosive index; VEI; 6) eruptions known from the AVZ (Stern et al., 2011; Fontijn et al., 2014). Tephra from this eruption was previously identified in the stratigraphy of Hooker's Point (HP05 sequence) by Monteath et al. (2019).

3.1.2. Monte Burney

Cryptotephra deposits PP_176–177 and CC_521–522, in the Pond Point and Cape Carysfort sequences, are formed of abundant clear, cuspate and vesicular shards, with high SiO_2 (avg. 77.58 wt% and 77.58 wt%) and low K_2O (avg. 1.82 and 1.89 wt%) values compared with other cryptotephra deposits in the Falkland Islands (Fig. 3, Table 2). The 2σ age ranges are 9700–9440 cal yr BP (CC_521–522) and 10,150–9700 cal yr BP (PP_176–177) and the cryptotephra deposits can be correlated between sites using major-minor-trace element compositions (Fig. 5, Table 3). A minor offset in Al_2O_3 wt% values is evident between PP_176–177 (avg. 12.90 wt%) and CC_521–522 (avg. 12.69 wt%) which likely reflects variations between analytical instruments. Two distinct glass populations are evident in both PP_176–177 and CC_521–522 and are discussed below.

The major-minor element compositions of PP_176–177 and CC_521–522 closely resemble tephra deposits in Hooker's Point (HP05_67) and Laguna Potrok Aike (PAS-2T1, LPA-12.32), in southernmost Patagonia, previously linked with the Early Holocene Monte Burney MB1 eruption (Fig. 5; Wastegård et al., 2013; Monteath et al., 2019; Smith et al., 2019). However, while a link between medial-distal Monte Burney deposits from southern Patagonia (note that 'proximal' deposits of Stern, 2008; Del Carlo et al., 2018 are all ~60–300 km from Monte Burney) and tephra deposits in the Falkland Islands and Laguna Potrok Aike appears robust, close inspection of existing data raises questions about which Patagonian units truly represent the MB1 eruption.

Major-minor element data from Stern's (2008) reference 'MB1' medial-distal deposits (MB1-BF-370; MB1-93-21W; MB1-TOM-GOLD), analysed by Smith et al. (2019), do not correlate with data from the Falkland Islands cryptotephra deposits (PP_176–177, CC_521–522, HP05_67) or the Laguna Potrok Aike 'MB1' tephra (PAS-2T1, LPA-12.32; Fig. 5). Instead, data from these 'MB1' reference samples (with one potential exception - Route-257) are indistinguishable from a thinner (0.2 cm thick) tephra deposit (LPA-12.51) in Laguna Potrok Aike that closely underlies the thicker (1.5 cm) overlying 'MB1' tephra (PAS-2T1, LPA-12.32; Wastegård et al., 2013; Smith et al., 2019). This more discreet deposit is referred to as the MBK1/2 tephra by Smith et al. (2019), following Kilian et al. (2003). Del Carlo et al. (2018) also reported an older Monte Burney tephra (AR-1B; 2.5 cm thick) at Arroyo Robles (11 km north from Laguna Potrok Aike), directly below a thicker MB1 deposit (AR-1D; 10–12 cm thick); consistent with observations in Laguna Potrok Aike (Smith et al., 2019). Note that data from the 'MB1' Route-257 sample (#14 in Stern, 2008; Smith et al., 2019) can be separated from all other MB1 references samples, with higher SiO_2 and lower Al_2O_3, and likely represent a different eruption.

Major-minor element MB1 data reported by Del Carlo et al. (2018) differ from those of Wastegård et al. (2013), Monteath et al. (2019), Smith et al. (2019) and this study, with higher SiO_2 wt% and lower Na_2O wt% values (Fig. 5). More stable elements (e.g., FeO_T and CaO) closely overlap with data from the thicker 'MB1' tephra in Laguna Potrok Aike (Laguna Potrok Aike (PAS-2T1, LPA-12.32) and the Falkland Islands Monte Burney cryptotephra (PP_176–177, CC_521–522, HP05_67), but are clearly offset with data from Stern's (2008) localities, analysed by Smith et al. (2019). Trace element data presented by Del Carlo et al. (2018) also show good overlap with the Falkland Islands Monte Burney cryptotephra, although there are some minor differences that likely reflect instrumental variability (Fig. 5). It seems likely that the terrestrial

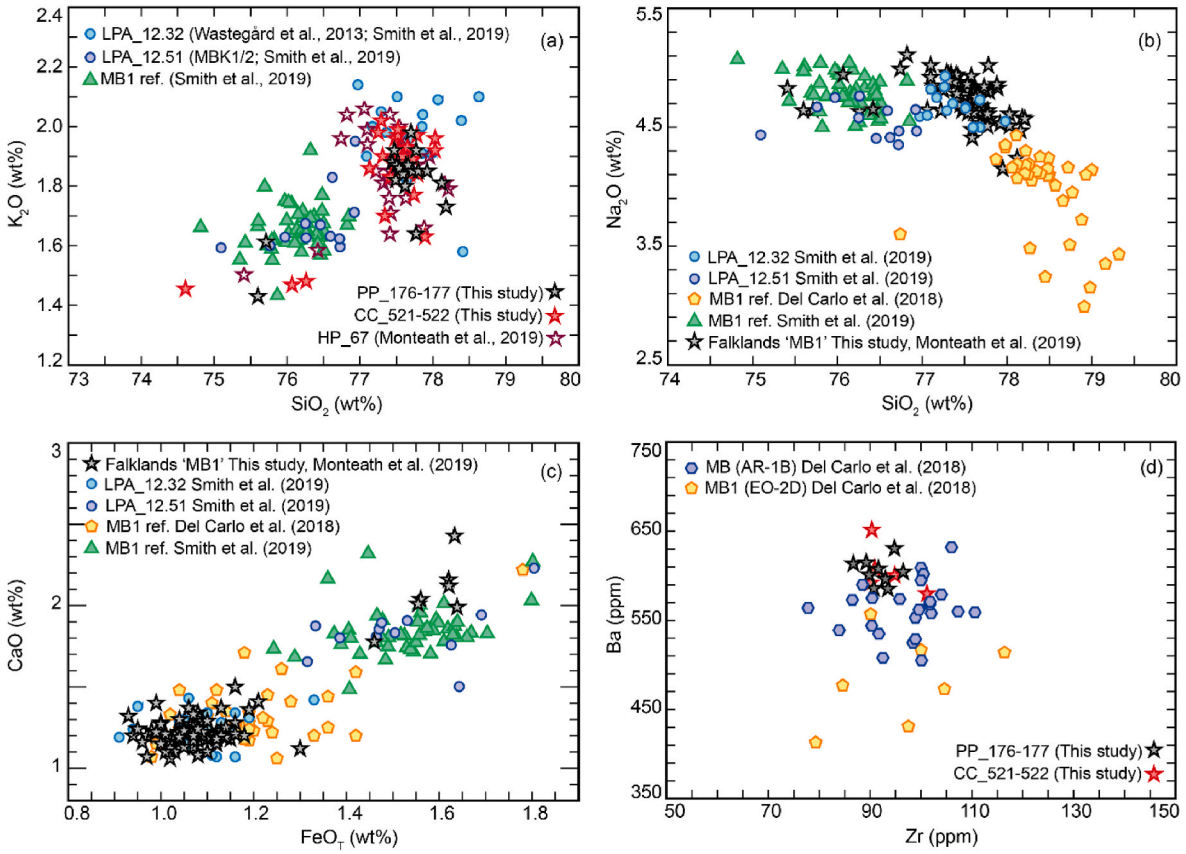

Fig. 5. Major and trace element biplots comparing volcanic glass data from the Falkland Islands cryptotephra medial deposits attributed Monte Burney.

MB1 deposits analysed by Del Carlo et al. (2018) can be correlated with the thicker 'MB1' tephra in Laguna Potrok Aike and the Falkland Islands MB1 cryptotephra deposits, however, major-minor element data are affected by Na_2O loss, either during EPMA or as a result of post-depositional weathering.

The geochemical disparity between the continental MB1 reference samples is challenging to interpret, and we cannot completely discount the possibility that this is the result of instrumental differences. The chronologies of Lake Potrok Aike and sampled terrestrial sections are also insufficiently resolved to differentiate Early Holocene eruptions. However, clustering of two separate 'MB1' geochemical populations, which largely distinguish the Del Carlo et al. (2018) and Stern (2008) deposits, combined with close association of two tephra layers in Laguna Potrok Aike which reflect the two separate 'MB1′ geochemical groupings, suggests these are real chemical offsets associated with different eruptive events. Together, this shows that tephra from two Early Holocene eruptions of Monte Burney is widely deposited across southernmost Patagonia and the Falklands Islands. Cryptotephra deposits in the Falkland Islands show strongest affinity with the younger, thicker Monte Burney tephra deposit described as MB1 in Laguna Potrok Aike (PAS-2T1; LPA-12.32), that may be linked with medial-distal deposits analysed by Del Carlo et al. (2018). However, a limited number of shards plot more closely with the older, thinner Monte Burney tephra deposit in Laguna Potrok Aike (LPA-12.31), that correlates with medial-distal deposits analysed by Smith et al. (2019), suggesting both glass populations may be present in the Falkland Islands.

The results show that the medial Monte Burney tephra deposits used as reference material for MB1 (MB1-BF-370; MB1-93-21W; MB1-TOM-GOLD) by Smith et al. (2019) may actually represent an underling tephra from the same source. Our study raises uncertainties surrounding the Early Holocene tephrostratigraphy of Monte Burney and highlight the importance of integrating near-source and distal records; particularly as the medial-distal study sites of Del Carlo et al. (2018) and Smith et al. (2019) are often closely spaced (Fig. 1) and would be expected to preserve the same tephrostratigraphy.

3.1.3. *Hudson volcano*

Cryptotephra deposits PP_89–90, CC_199–200 and HP05_212–213, in Pond Point, Cape Carysfort and Hooker's Point are comprised of abundant (concentrations vary from >80,000–200,000 shards per gram), clear, cuspate and platy shards with relatively low SiO_2 (68.74–69.00 wt%) and intermediate K_2O (3.47–3.62 wt%) values compared with other cryptotephra deposits in the Falkland Islands (Fig. 3, Table 2). A small component of light brown shards is also present. The relatively low SiO_2 content makes these deposits distinct from other cryptotephras in the Falkland Islands and tephras from the AVZ (e.g., Mt. Burney, Reclus and Aguilera; Fig. 3). Major-minor-trace elements from PP_89–90, CC_199–200 and HP05_212–213 closely match with the Hudson volcano H2 tephra and can be correlated with this eruption (Fig. 6). There is an offset in Al_2O_3 values from CC_199–200 (Fig. 6), which again likely reflects instrumental variability as the major-minor elements of cryptotephra deposits PP_89–90, CC_199–200 and HP05_212–213 were measured in different laboratories, using different instruments. However, trace-element data from the same laboratory

Table 3
Mean and standard deviation glass trace-element geochemistry for Falkland Islands cryptotephra deposits.

Source	Sample	n	Rb	Sr	Y	Zr	Nb	Ba	La	Ce	Pr	Nd	Sm	Eu	Gd	Dy	Er	Yb	Lu	Hf	Ta	Th	U
Hudson	PP_89-90	7	100.37	149.86	45.36	511.50	22.84	923.60	49.33	107.82	12.14	48.18	9.79	2.00	7.85	8.16	5.01	5.52	0.80	11.85	1.23	9.57	2.40
			10.69	4.41	1.26	17.40	0.43	34.95	1.75	3.26	0.48	2.18	0.37	0.17	0.40	0.45	0.31	0.26	0.05	0.65	0.05	0.28	0.11
	CC_199-200	9	96.80	156.04	45.20	509.58	23.11	945.75	48.92	109.23	12.38	48.92	9.88	2.04	7.90	7.83	4.91	5.26	0.81	11.47	1.21	9.64	2.47
			1.57	8.49	2.53	24.03	0.98	43.88	2.90	6.14	0.53	3.23	0.89	0.10	0.59	0.64	0.57	0.64	0.07	1.53	0.08	0.72	0.26
Aguilera	CC_241-242	16	135.86	129.03	6.76	83.63	13.64	740.85	31.13	53.45	4.72	14.14	2.93	<LOD	<LOD	<LOD	<LOD	<LOD	<LOD	2.84	1.45	21.94	5.45
			3.86	4.96	0.32	5.45	0.42	37.92	1.61	2.47	0.28	0.67	1.16	<LOD	<LOD	<LOD	<LOD	<LOD	<LOD	0.44	0.09	1.45	0.31
Unknown	CC_255-256	8	172.15	90.91	25.60	153.80	11.10	771.23	29.51	61.49	6.70	26.16	4.87	0.67	4.42	4.50	2.72	2.96	0.44	4.61	0.90	16.73	4.53
			45.88	38.86	14.94	63.15	1.84	123.08	3.06	6.74	1.14	5.81	1.94	0.21	2.01	2.55	1.68	1.46	0.26	1.57	0.12	3.12	0.86
Chaitén	CC_278-279	14	145.02	102.86	15.55	90.25	11.05	656.19	26.92	52.41	5.32	18.20	3.39	0.53	2.71	2.64	1.68	1.90	0.27	2.96	1.00	14.29	3.94
			35.81	36.50	10.45	31.41	4.05	59.61	4.48	10.18	1.34	5.65	1.54	0.11	1.34	1.65	1.26	1.20	0.17	0.89	0.32	3.23	0.55
Monte Burney	CC_521-522	5	30.12	174.36	11.36	93.45	6.34	606.44	14.93	31.40	3.38	14.14	2.59	0.50	2.00	2.10	1.28	1.40	0.22	3.07	0.46	2.44	0.78
			1.62	9.65	0.45	4.73	0.30	27.27	0.45	0.75	0.28	1.24	0.34	0.12	0.42	0.34	0.27	0.22	0.04	0.25	0.03	0.21	0.12
	PP_176-177	9	31.59	166.91	11.52	91.75	6.27	604.41	14.84	30.99	3.41	13.28	2.70	0.55	2.19	1.94	1.25	1.46	0.21	3.16	0.47	2.55	0.75
			1.35	3.54	0.28	3.02	0.18	14.48	0.26	0.77	0.16	0.85	0.24	0.07	0.44	0.15	0.13	0.22	0.02	0.24	0.02	0.19	0.06
Reclus	HP20_12_13	11	58.53	229.91	12.79	92.01	11.59	782.22	27.56	54.11	5.54	20.43	3.67	0.71	2.70	2.24	1.33	1.46	0.19	2.91	0.89	5.91	1.84
			5.68	12.66	0.43	15.83	0.46	31.61	1.13	1.96	0.30	0.69	0.22	0.07	0.40	0.33	0.13	0.15	0.03	0.31	0.04	0.42	0.12

support the correlation between PP_89–90 and CC_199–200. The H2 tephra has previously been identified in the East Falkland in the Canopus Hill peat sequence (cryptotephra deposit CP_139) by Panaretos et al. (2021). The identification of H2 tephra in three additional sites in this study confirms that H2 is a widespread marker across the Falkland Islands.

Discrete sub-populations of volcanic glass likely derived from Hudson volcano based on its distinctive glass compositions (relative to other regional volcanoes) are also present in several samples from Hooker's Point and Cape Carysfort (HP05_25–26, HP05_3–4, CC_142–143). These may represent reworked H2 material, or tephra from Late Holocene or historical eruptions of Hudson Volcano (e.g., Haberle and Lumley, 1998).

3.1.4. *Aguilera volcano*

Three cryptotephra deposits in the Falkland Islands show a strong affinity with the A1 tephra from Aguilera volcano (Fig. 6; Table 1). Cryptotephra deposits CC_241–242, HP05_289–290 and HP05_224–228 in Cape Carysfort and Hooker's Point are all formed of abundant (>30,000–5000 shards per gram), clear, cuspate and platy shards, with high SiO_2 (avg. 77.64, 77.83 and 77.46 wt%) and high K_2O (avg. 4.20, 4.08 and 4.00 wt%) values compared with other cryptotephra deposits in the Falkland Islands (Fig. 3, Table 2). These Aguilera tephras have low FeOt (0.90–0.96 wt%) and Na_2O (3.32–3.45 wt%) compared with other AVZ tephra deposits. CC_241–242 has slightly lower Al_2O_3 wt% values than the other Aguilera-type cryptotephra deposits in the Falkland Islands, however, this is also reflected in the secondary standards and is likely caused by analytical variation (Table S3). CC_241–242 and HP05_224–228 can be correlated with each other based on their age and stratigraphic position and are informally referred to as Aguilera Falkland's Tephra One (AF1), while HP05_289–290 is likely to represent an older eruption from the same source. Trace element data for AF1 (CC_241–242) cannot be compared with proximal Aguilera deposits as to our knowledge no single-grain trace-element glass data exists (Table 3).

While the major-minor element data for AF1 are a good match with Aguilera (Fig. 6.), the modelled ages of the Falkland Islands cryptotephra deposits (CC_241–242, 4280 ± 65 cal yr BP; HP05_224–228, 4180 ± 140 cal yr BP) are older than age estimates for the widespread A1 tephra. Stern (2008) reported a widely cited age of 3070–3400 cal yr BP for the A1 eruption using bracketing radiocarbon ages, however, the chronology of A1 is founded on dates of mixed quality and materials. Only three of the dates reported by Stern (2008) are incompatible with our modelled ages for AF1 and these may well not be reliable because of unclear stratigraphic relationships and choice of materials for dating (e.g., acid fractions). More recent radiocarbon dating from Santa Cruz River at the Río Bote 1 archaeological site provide evidence for an older widespread eruption of Aguilera that may in fact be the A1 tephra. Franco et al. (2017) report bracketing dates from charcoal and human skeletal remains, as well as charcoal from inside a bone tool within an Aguilera tephra, that was deposited 4410–4160 cal yr BP (dates recalibrated using SHCal20; Hogg et al., 2020). This older age is in good agreement with our modelled age of AF1 and could suggest that AF1 and A1 may be correlated. The A1 tephra was distributed eastward, towards the Falkland Islands, and it seems surprising that ash from this large (≥3.6 km^3; Stern, 2008) eruption would not be present in the archipelago, but tephra from smaller eruptions of Aguilera were. We therefore suggest that AF1 is likely to correlated with A1 and that the true age of the A1 eruption is ca. 4200 cal yr BP. Careful radiocarbon dating and glass major-minor-trace element analyses should be undertaken to test our hypothesis.

Cryptotephra deposit HP05_289–290 underlies AF1 and is likely to represent an older eruption from the same source that took place 5720 ± 240 cal yr BP. Whilst the A1 eruption is the most widely described Aguilera eruption, several thinner and less extensively distributed tephra deposits have been linked with Aguilera in southern South

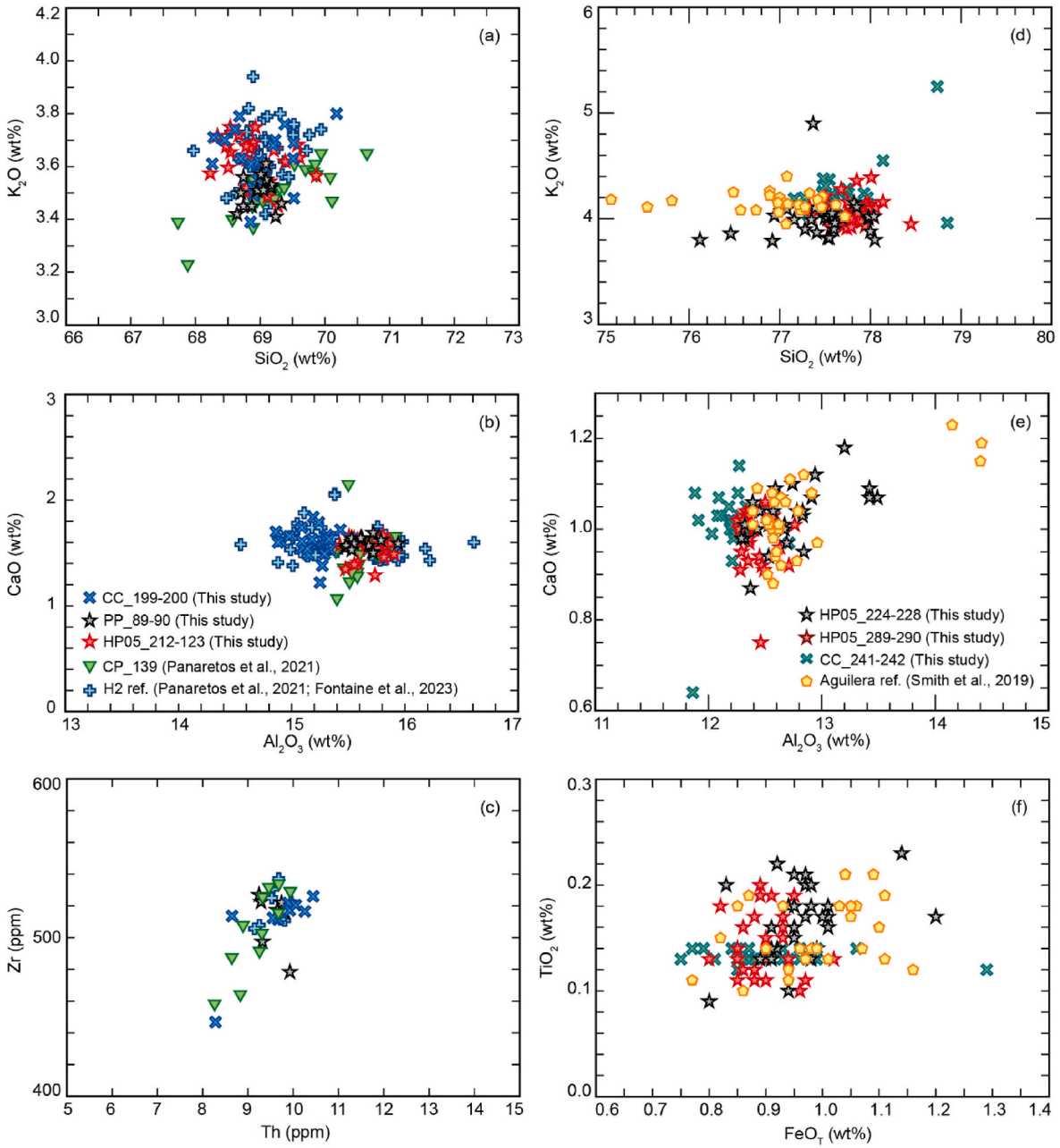

Fig. 6. Major-minor-trace element biplots comparing glass EPMA and LA-ICP-MS data from the Falkland Islands with data from Hudson H2 (a,b,c) and Aguilera A1 (d,e,f).

America; although no glass geochemical data are available from these deposits to our knowledge. Stern (2008) summarise radiocarbon evidence for reported Aguilera tephra beds older than the A1. The strongest evidence comes from Villa-Martínez and Moreno (2007) who report two Mid Holocene tephra deposits linked with Aguilera in peat cores from the Torres del Paine area, dated to between 5700 and 5150 cal yr BP. It is likely that HP05_289–290 corresponds to a smaller, Mid Holocene eruption of Aguilera volcano, however, further work in near-source and medial settings is required to test this hypothesis.

3.1.5. *Chaitén volcano*

Cryptotephra deposits CC_278–279 in Cape Carysfort and HP05_258–259 in Hooker's Point (HP05) are comprised of abundant (>30,000 shards per gram), clear, cuspate, platy glass shards, with high SiO_2 values (avg. 76.00, 76.31 wt%) and intermediate K_2O values (avg. 3.07, 2.96 wt%) compared with other cryptotephra deposits in the Falkland Islands (Fig. 3, Table 2). The 2σ age ranges of CC_278–279 and HP05_258–259 are 5210–4480 and 5280–4880 cal yr BP and these cryptotephra deposits can be correlated with one and other. There is a minor offset in Al_2O_3 wt% values between CC_278–279 and HP05_258–259 which likely reflects instrumental variation as these

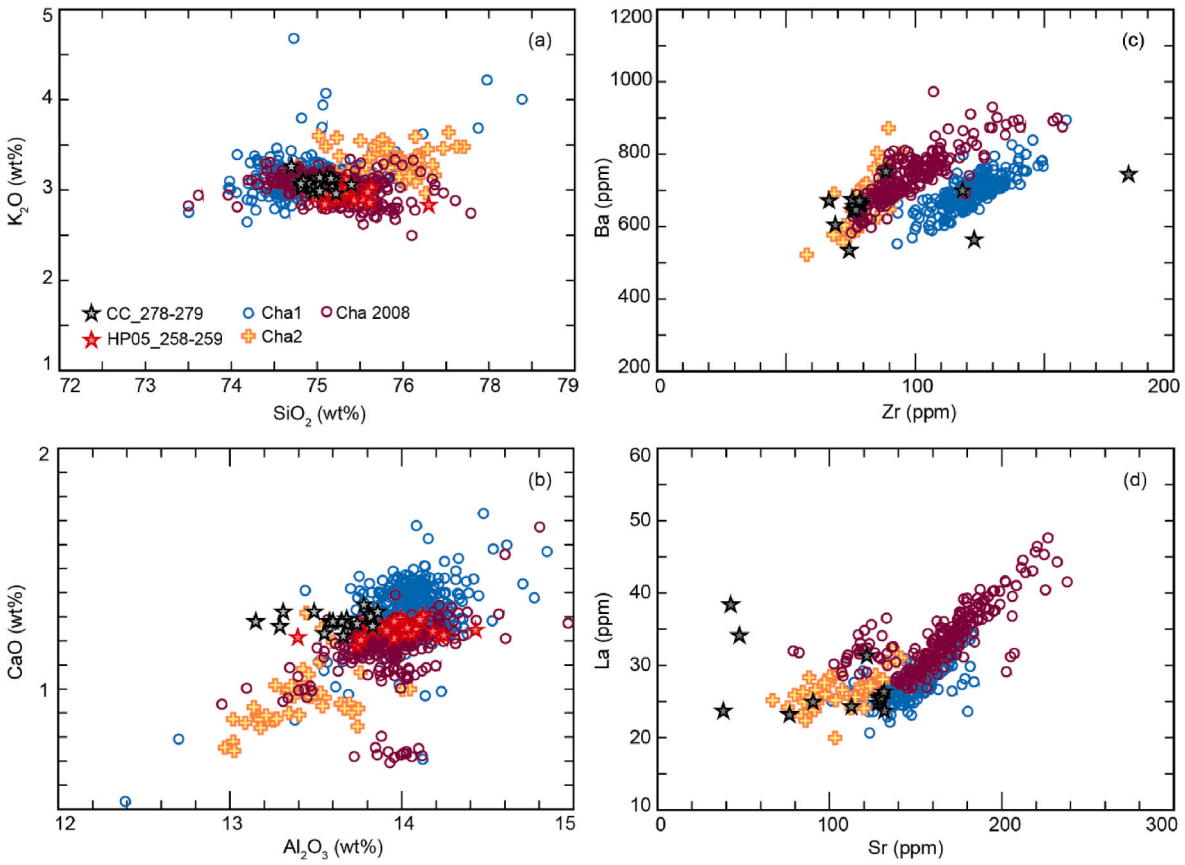

Fig. 7. Major-minor-trace element biplots comparing glass EPMA and LA-ICP-MS data from the Falkland Islands with data from Chaitén volcano (Fontaine et al., 2023; references therein).

were run on different instruments (Fig. 7).

Major-minor element data from both CC_278–279 and HP05_258–259 show strong similarities with tephra deposits from Chaitén volcano, in central Chile (Fig. 6). In particular, major-minor elements from CC_278–279 and HP05_258–259 are almost identical to tephra from the Cha-1 eruption (9900 ± 250 cal yr BP; Fontijn et al., 2016) and the historical VCha-2008 eruption from Chaitén volcano. Trace element values from Cha-1 eruption and VCha-2008 also show strong similarities with CC_278–279, however, can be differentiated (Fig. 7). Curiously, the reported ages of these eruptions are very different to the modelled ages of the Falkland Islands cryptotephra deposits and this precludes a correlation. The CC_278–279 and HP05_258–259 deposits have an integrated age of 5035 ± 105 cal yr BP (Fig. 8), which is in good agreement with the Cha-2/Pumalin tephra from Chaitén volcano (5013 ± 111 cal yr BP; Watt et al., 2013; Alloway et al., 2017). The Cha-2/Pumalin tephra is one of the largest-volume Holocene eruptions of Chaitén and is likely to have a widespread distribution. However, whilst it is a good chronological match there are differences between the major-trace-element compositions of Cha-2/Pumalin and the Falkland Islands cryptotephra deposits. Given the strong affinity of CC_278–279 and HP05_258–259 to other Chaitén deposits (VCha-2008 and Cha-1) these cryptotephra deposits are very likely to originate from Chaitén and represent the most distal identification of Chaitén tephra to date (>1400 km from source). However, a correlation to a specific event cannot be made at this point.

3.1.6. *Uncorrelated cryptotephra deposits*

Cryptotephra deposit CC_255–256 in Cape Carysfort is formed of abundant (~50,000 shards per gram) clear shards, with intermediate SiO_2 (avg. 74.10 wt%) and high K_2O (avg. 4.11 wt%) values relative to other cryptotephra deposits in the Falkland Islands (Fig. 3, Table 2). The 2σ age range of CC_255–256 is 4460–4200 cal yr BP. Major-minor elements from CC_255–256 show some similarities to samples from Volcan Sollipulli and the So-A eruption, from the same source, which has been identified in Diamond Bog, South Georgia (Oppedal et al., 2018). However, there are substantial offsets in CaO and FeOt values (Fig. 7) that preclude any correlation and the source of CC_255–256 remains unclear. There are also offsets between major-minor element data from the So-A eruption and the Diamond Bog cryptotephra deposit, and this correlation should be tested further (Fig. 8).

Cryptotephra deposit HP05_107–108 in Hooker's Point, is formed of abundant (>6000 shards per gram), clear, cuspate shards. The deposit is mostly formed of detrital glass; however, a discrete sub-population is present with low SiO_2 (avg. 72.18 wt%) and intermediate K_2O (avg. 2.67 wt%) values relative to other cryptotephra deposits in the Falkland Islands (Fig. 3, Table 2). The 2σ age range of HP05_107–108 is 2380–1770 cal yr BP. Major-minor elements from the HP05_107–108 sub-population are indistinguishable from the Playas Blancas Negras tephra from the Antillanca volcanic complex in central Chile (Fig. 8). This tephra was produced during a large eruption (VEI 5) between 2280 and 2200 cal yr BP and has been identified in multiple records throughout the Chilean Lake District (Fontijn et al., 2016). At present, the limited number of consistent EPMA data precludes correlation between HP05_107–108 and the Playas Blancas Negras tephra, but other distal sites with less substantial detrital input may confirm this.

3.2. *Revised ages of key isochrons*

Our chronological approach exploits the benefits of Bayesian age modelling within multiple stratigraphically constrained sequences of

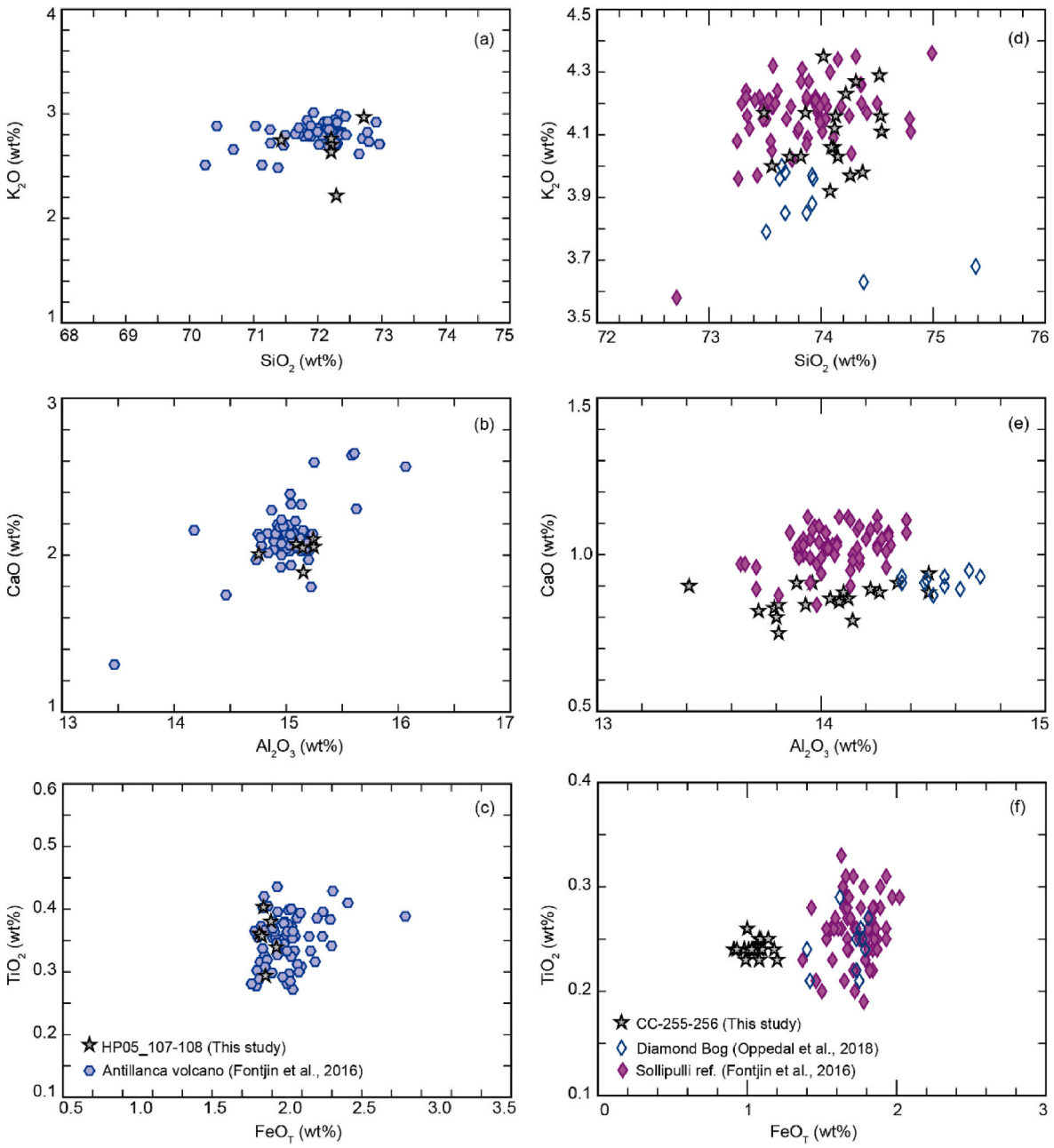

Fig. 8. Major-minor element biplots comparing glass EPMA data from the Falkland Islands with data from Antillanca volcano and Volcan Sollipulli.

radiocarbon ages from distal depositional environments. This approach has been shown to be effective in generating reliable age estimates for tephra isochrons identified in both distal and proximal settings (e.g., Pizer et al., 2023). In the Falkland Islands peat-cores, it also helps to mitigate for vertical reworking that can obscure the true stratigraphic position of the isochron. Like all depositional settings, the Falkland Islands peatlands are affected by well-known post depositional processes (e.g., fluctuating water-tables, root penetration and bioturbation; Payne et al., 2005, Payne and Gehrels, 2010; Watson et al., 2015; Mackay et al., 2016) that produce 'tails' of tephra extending upward and downward from the isochron (Fig. 2). As the concentrations of tephra are so high in the Falklands peat-records (often >50,000 shards per gram), which are also continually affected by reworked detrital glass from Patagonia (Monteath et al., 2019), the stratigraphic position of isochrons can only be constrained with 4–5 cm accuracy in some cases (e.g., Hudson H2; Fig. 2). By using stratigraphic and chronological data from multiple sequences this uncertainty is largely negated.

3.2.1. *R1 tephra*

The age of the R1 tephra has been constrained with 17 additional radiocarbon dates to the previously published Hooker's Point sequence. By integrating these ages, we have constrained the age of the R1 tephra to ca.14,280 cal yr BP (2σ range of 14,800–14,060 cal yr BP). The new age reported here is in good agreement with previously reported ages from Smith et al. (2019) (14,500–14,100 cal yr BP) and Stern et al. (2011) (14,760 ± 180 cal yr BP), but marginally younger than the age of ~15,000 cal yr BP suggested by McCulloch et al. (2024) (Figs. 9 and 10; Table 4). The R1 tephra has the potential to be used as an isochron to mark the onset of the Antarctic Cold Reversal; a cooling event spanning ~14,700–13,000 cal yr BP that is widely expressed in the Antarctic ice cores, in Patagonia, and across the Southern Oceans (Moreno et al., 2009; Pedro et al., 2016).

3.2.2. *Monte Burney deposit*

While there is uncertainty surrounding the Early Holocene

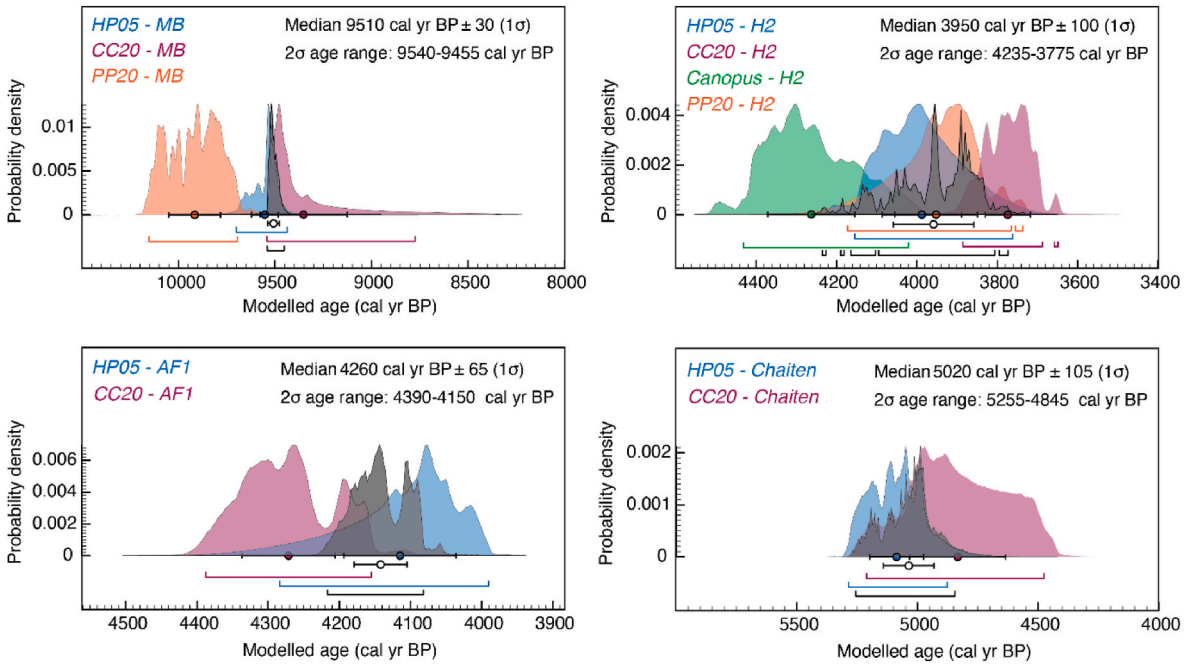

Fig. 9. Integrated ages for the H2, MB, AF1, and Chaitén distal tephra deposits in the Falkland Islands. Coloured solid lines below each plot indicate the 2σ age range (95.4 % of the probability distribution) from the independent age estimates from each core, black solid lines indicate the 2σ age range from the linked P_sequence.

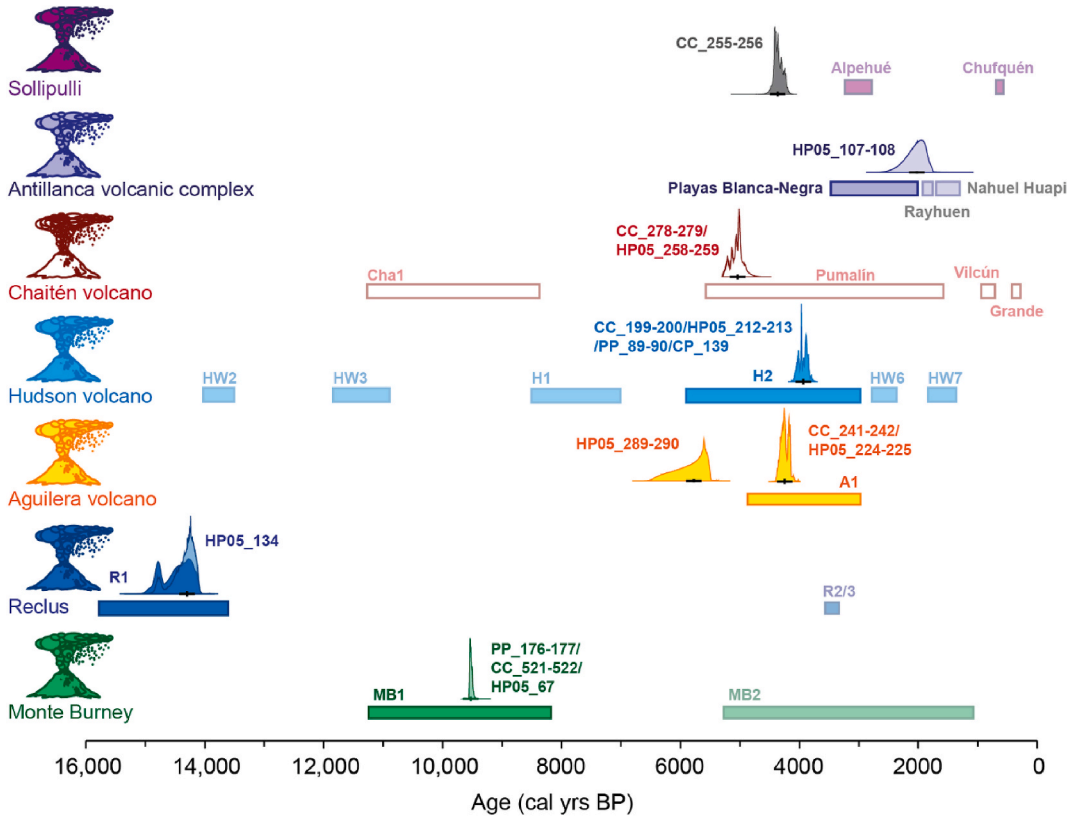

Fig. 10. Modelled probability distributions for each of the tephra deposits identified in this study plotted against the eruptive history of the seven volcanoes discussed in the text (Fontaine et al., 2023; references therein). Where tephra deposits were identified in multiple Falkland Islands peat-cores output from the integrated OxCal age-depth model is presented.

tephrostratigraphy of Monte Burney MB1 (see section 3.1.2), it is clear that an Early Holocene tephra deposit from Monte Burney is found across the Falkland Islands. The integrated median age for the Falkland Islands Monte Burney cryptotephra using Hooker's Point, Cape Carysfort and Pond Point, is ca. 9510 cal yr BP (with a 2σ age range of 9540–9455 cal yr BP). The Hooker's Point and Cape Carysfort

Table 4
Summary of integrated ages and previous ages for key tephra isochrons. Where possible, ages have been recalibrated using SHCal20 (Hogg et al., 2020) and are reported at two-sigma (95.4 %) uncertainty.

Tephra	Source volcano	VEI	Age estimate (cal yr BP)	References
R1	Reclus volcano	6	**14,800-14,060**	**Integrated median age; this study**
			14,500–14,100	Smith et al. (2019)
			15,680–14,090	Stern et al. (2011)
			15,230–14,555	McCulloch et al. (2005)
			~15,000	McCulloch et al. (2024)
MBK1	Monte Burney		10,600 - 10,200	Smith et al. (2019)
MB1[a]	Monte Burney	5	9540-9455	**Integrated median age; this study**
			10,400–10,000	Smith et al. (2019)
			10,490–9190	Monteath et al. (2019)
			10,650–10,250, 8190-7980	Del Carlo et al. (2018)
			10,720-8200	Stern (2008)
			9180–9000	Kilian et al. (2003)
Unclear	Chaitén volcano		5255-4845	**Integrated median age; this study**
Pumalin tephra	Chaitén volcano		5590–4630	Alloway et al. (2017)
Cha-2	Chaitén volcano		5040–4860	Watt et al. (2013)
AF1	Aguilera volcano		4390-4150	**Integrated median age; this study**
Unnamed	Aguilera volcano		4410–4160	Franco et al. (2017)
A1		5	3370–2870	Stern (2008)
H2	Hudson volcano	6	4235-3775	**Integrated median age; this study**
			<4790-4410	Zanchetta et al. (2021)
			4265 ± 65	Panaretos et al. (2021)
			3870 ± 240	Weller et al. (2018)
			4110–3970	Van Daele et al. (2016)
			~3900	Naranjo and Stern (1998)

[a] Note that the Early Holocene Monte Burney cryptotephra deposits in the Falkland Islands may not represent the MB1 eruption.

independent age models fall within this range, while the age estimate from Pond Point is slightly older. The age of the Falklands Monte Burney cryptotephra is marginally younger than LPA-12.32 in Laguna Potrok Aike, with which it is correlated based on major-minor element analyses (Smith et al., 2019) (Figs. 9 and 10; Table 4). However, radiocarbon dates from Laguna Potrok Aike are derived from the remains of aquatic mosses, which may include old carbon, and so a slight age offset is not unexpected (Kliem et al., 2013). If the correlation between MBK1/2 and medial MB1 tephra deposits is correct then the Falkland Islands Monte Burney cryptotephra provides a minimum age estimate for MB1 which is poorly constrained, with several different (but overlapping) dates (Table 4).

3.2.3. H2 tephra

The integrated age from four peat sequences on the Falkland Islands (Hooker's Point, Cape Carysfort, Pond Point and Canopus Hill) suggests a median age of 3950 cal yr BP (4230–3775 cal yr BP) for the H2 eruption of Hudson volcano. This is slightly younger than the age reported in Panaretos et al. (2021) but is in good agreement with previous age ranges from the South American mainland (Figs. 9 and 10; Table 4).

4. Conclusions

The identification of the Monte Burney and Hudson volcano cryptotephra deposits from the far east of the Falkland archipelago (Cape Carysfort, Hooker's Point and previously at Canopus Hill) to the far west in the Pond Point sequence on Weddell Island, demonstrates archipelago-wide deposition of tephra from these events. Our integrated Bayesian age-depth model refines the median ages of key isochrons including the Hudson (H2), an Early Holocene Monte Burney eruption and the Reclus (R1) cryptotephra deposits in the Falkland Islands. The discovery of volcanic glass from multiple Aguilera eruptions and glass compositions consistent with Chaitén and Antillanca volcanoes, greatly increases the previously known distribution of tephra from these sources. Many of the Falkland cryptotephra deposits now represent the most distal identifications of tephra from their respective source volcanoes/eruptions. However, our distal research also highlights uncertainties and areas that require further investigation in near source settings; notably uncertainties surrounding the age of the A1 and other Mid Holocene eruptions of Aguilera volcano, as well as the possibility that two Early Holocene tephras from Monte Burney are widespread in southernmost Patagonia. This highlights the value of integrating near-source and distal tephrostratigraphic information when reconstructing pre-historic volcanism and the associated ash dispersal. The high concentrations of glass shards in the Falkland Islands suggests that many of these cryptotephras may be more widespread than presently understood and reinforces possibilities for correlations in ultra-distal settings such as Antarctic ice cores, sediments on sub-Antarctic islands, and marine sediments in the Southern Ocean. Finally, our reference dataset of major-minor-trace element glass composition is an important contribution to the regional tephrostratigraphic framework that will aid near source and distal correlations.

Author contributions

P. Panaretos: conceptualization, methodology, investigation, data collection and analysis, writing original draft. **A. J. Monteath**: conceptualization, methodology, investigation, data collection and analysis, writing original draft. **Z. A. Thomas**: conceptualization, methodology, investigation, data collection and analysis, writing original draft; funding acquisition. **P. G. Albert:** methodology, data collection and analysis, writing reviewing and editing; funding acquisition. **B. J.L Jensen**: data collection and analysis, methodology, writing reviewing and editing. **J. Tamhane**: data collection and analysis. **S. Woudstra**: data collection and analysis, editing. **G. Jones**: data collection and analysis. **R. Scaife**: sample collection and funding acquisition. **M.J. Bentley**: sample collection, editing.

Declaration of competing interest

We declare that there are no conflicts of interest regarding this manuscript. None of this material has been published previously or is under consideration elsewhere, and all authors have approved submission of the final manuscript.

Acknowledgements

This project was supported by the Australian Research Council (DE200100907 awarded to Zoë Thomas). Paul G Albert and Gwydion Jones were funded through a UKRI Future Leaders Fellowship (MR/S035478/1; MR/Y011767/1) awarded to P G Albert. We thank the Falkland Islands Government and local landowners for permission to undertake sampling on the island. We thank A. Long and P. Stone for access to the 2005 Hooker's Point peat core. The Shackleton Trust and the Falkland Islands Department of Mineral Resources supported 2005 Hooker's Point field work. We thank Prof. Victoria Smith and Dr Chris Hayward for assistance with the electron microprobe analyses, and Dr

Christina Manning for assistance with the LA-ICP-MS analysis.

Appendix A. Supplementary data

Supplementary data to this article can be found online at https://doi.org/10.1016/j.quascirev.2025.109599.

Data availability

All data and/or code is contained within the submission.

References

Alloway, B.V., Pearce, N.J., Moreno, P.I., Villarosa, G., Jara, I., De Pol-Holz, R., Outes, V., 2017. An 18,000 year-long eruptive record from volcán Chaitén, northwestern Patagonia: paleoenvironmental and hazard-assessment implications. Quat. Sci. Rev. 168, 151–181.

Blockley, S.P.E., Pyne-O'Donnell, S.D.F., Lowe, J.J., Matthews, I.P., Stone, A., Pollard, A. M., Turney, C.S.M., Molyneux, E.G., 2005. A new and less destructive laboratory procedure for the physical separation of distal glass tephra shards from sediments. Quat. Sci. Rev. 24 (16–17), 1952–1960. https://doi.org/10.1016/j.quascirev.2004.12.008.

Bronk Ramsey, C., 2008. Deposition models for chronological records. Quat. Sci. Rev. 27, 42–60. https://doi.org/10.1016/j.quascirev.2007.01.019.

Bronk Ramsey, C., 2009. Dealing with outliers and offsets in radiocarbon dating. Radiocarbon 51, 1023–1045. https://doi.org/10.1017/S0033822200034093.

Bronk Ramsey, C., Lee, S., 2013. Recent and planned developments of the program OxCal. Radiocarbon 55, 720–730. https://doi.org/10.2458/azu_js_rc.55.16215.

Del Carlo, P., Di Roberto, A., D'Orazio, M., Petrelli, M., Angioletti, A., Zanchetta, G., Maggi, V., Daga, R., Nazzari, M., Rocchi, S., 2018. Late Glacial-Holocene tephra from southern Patagonia and Tierra del Fuego (Argentina, Chile): a complete textural and geochemical fingerprinting for distal correlations in the Southern Hemisphere. Quat. Sci. Rev. 195, 153–170. https://doi.org/10.1016/j.quascirev.2018.07.028.

Donovan, J.J., Kremser, D., Fournelle, J.H., Goemann, K., 2015. In: Probe for EPMA: Acquisition, Automation and Analysis, Version 11: Eugene, Oregon. Probe Software. Inc.. http://www.probesoftware.com

Dugmore, A.J., Larsen, G.R., Newton, A.J., 1995. Seven tephra isochrones in Scotland. Holocene 5 (3), 257–266.

Fontaine, C.M., Siani, G., Delpech, G., Michel, E., Villarosa, G., Manssouri, F., Nouet, J., 2021. Post–glacial tephrochronology record off the Chilean continental margin (~ 41° S). Quat. Sci. Rev. 261, 106928.

Fontaine, C.M., Peña-Araya, V., Marmo, C., Le Morvan, M., Delpech, G., Fontijn, K., Siani, G., Cosyn-Wexsteen, L., 2023. BOOM! tephrochronological dataset and exploration tool of the southern (33–46° S) and Austral (49–55° S) volcanic zones of the Andes. Quat. Sci. Rev. 316, 108254.

Fontijn, K., Rawson, H., Van Daele, M., Moernaut, J., Abarzúa, A.M., Heirman, K., Bertrand, S., Pyle, D.M., Mather, T.A., De Batist, M., Naranjo, J.A., 2016. Synchronisation of sedimentary records using tephra: a postglacial tephrochronological model for the Chilean Lake district. Quat. Sci. Rev. 137, 234–254. https://doi.org/10.1016/j.quascirev.2016.02.015.

Fontijn, K., Lachowycz, S.M., Rawson, H., Pyle, D.M., Mather, T.A., Naranjo, J.A., Moreno-Roa, H., 2014. Late Quaternary tephrostratigraphy of southern Chile and Argentina. Quat. Sci. Rev. 89, 70–84. https://doi.org/10.1016/j.quascirev.2014.02.007.

Franco, N.V., Brook, G.A., Guraieb, S.G., Mancini, M.V., Guarido, A.L., Mehl, A., Montenegro, T., 2017. Reuse of burial sites during the late Holocene: evidence from multiple human burials at the Río Bote 1 rockshelter, Upper Santa Cruz river basin (Southern Patagonia, Argentina). Lat. Am. Antiq. 28 (4), 476–494.

Global Volcanism Program, 2025. Smithsonian Institution. https://volcano.si.edu/. (Accessed 16 March 2025).

Groff, D.V., Hamley, K.M., Lessard, T.J., Greenawalt, K.E., Yasuhara, M., Brickle, P., Gill, J.L., 2020. Seabird establishment during regional cooling drove a terrestrial ecosystem shift 5000 years ago. Sci. Adv. 6 (43), eabb2788.

Haberle, S.G., Lumley, S.H., 1998. Age and origin of tephras recorded in postglacial lake sediments to the west of the southern Andes, 44°S to 47°S. J. Volcanol. Geoth. Res. 84, 239-256 https://doi.org/10.1016/S0377-0273(98)00037-7.

Hall, V.A., Wilson, P., Holmes, J., 2001. A preliminary tephra study of Holocene peats in the Falkland Islands. Dossiers de l'Archäol-Logis 1, 39–44.

Harlan, M.M., Fox, J., Kjær, H.A., Vance, T.R., Svensson, A., Cook, E., 2024. Cryptotephra in the east Antarctic Mount Brown South ice core. Clim. Past Discuss. [preprint], in review. https://doi.org/10.5194/cp-2024-64.

Hayward, C., 2012. High spatial resolution electron probe microanalysis of tephras and melt inclusions without beam-induced chemical modification. Holocene 22 (1), 119–125. https://doi.org/10.1177/0959683611409777.

Hogg, A.G., Heaton, T.J., Hua, Q., Palmer, J.G., Turney, C.S.M., Southon, J., Bayliss, A., Blackwell, P.G., Boswijk, G., Ramsey, C.B., Pearson, C., 2020. SHCal20 southern hemisphere calibration, 0–55,000 years cal BP. Radiocarbon 62 (4), 759–778. https://doi.org/10.1017/RDC.2020.59.

Hua, Q., Turnbull, J.C., Santos, G.M., Rakowski, A.Z., Ancapichún, S., De Pol-Holz, R., Hammer, S., Lehman, S.J., Levin, I., Miller, J.B., Palmer, J.G., 2021. Atmospheric radiocarbon for the period 1950–2019. Radiocarbon 64 (4), 723–745. https://doi.org/10.1017/RDC.2021.95.

Jensen, B.J., Davies, L.J., Nolan, C., Pyne-O'Donnell, S., Monteath, A.J., Ponomareva, V., Portnyagin, M., Booth, R., Bursik, M., Cook, E., Plunkett, G., 2021. Quat. Sci. Rev. 272, 107242.

Jochum, K.P., Stoll, B., Herwig, K., Willbold, M., Hofmann, A.W., Amini, M., Aarburg, S., Abouchami, W., Hellebrand, E., Mocek, B., Raczek, I., 2006. MPI-DING reference glasses for in situ microanalysis: new reference values for element con centrations and isotope ratios. G-cubed 7 (2). https://doi.org/10.1029/2005GC001060.

Kilian, R., Hohner, M., Biester, H., Wallrabe-Adams, H.J., Stern, C.R., 2003. Holocene peat and lake sediment tephra record from the southernmost Chilean Andes (53-55 degrees S). Rev. Geol. Chile 30 (1), 23–37. https://doi.org/10.4067/S0716-02082003000100002.

Klaes, B., Wörner, G., Kremer, K., Simon, K., Kronz, A., Scholz, D., Mueller, C.W., Höschen, C., Struck, J., Arz, H.W., Thiele-Bruhn, S., 2022. High-resolution stalagmite stratigraphy supports the late Holocene tephrochronology of southernmost patagonia. Commun. Earth Environ. 3 (1), 1–15.

Kliem, P., Enters, D., Hahn, A., Ohlendorf, C., Lisé-Pronovost, A., St-Onge, G., Wastegård, S., Zolitschka, B., PASADO Science Team, 2013. Lithology, radiocarbon chronology and sedimentological interpretation of the lacustrine record from Laguna Potrok Aike, southern Patagonia. Quat. Sci. Rev. 71, 54–69.

Koffman, B.G., Dowd, E.G., Osterberg, E.C., Ferris, D.G., Hartman, L.H., Wheatley, S.D., Kurbatov, A.V., Wong, G.J., Markle, B.R., Dunbar, N.W., Kreutz, K.J., Yates, M., 2017. Rapid transport of ash and sulfate from the 2011 Puyehue-Cord_on Caulle (Chile) eruption to west Antarctica. J. Geophys. Res. Atmos. 122, 8908–8920. https://doi.org/10.1002/2017JD026893.

Kuehn, S.C., Froese, D.G., Shane, P.A., 2011. The INTAV intercomparison of electron-beam microanalysis of glass by tephrochronology laboratories: results and recommendations. Quat. Int. 246, 19–47. https://doi.org/10.1016/j.quaint.2011.08.022.

McCulloch, R.D., Bentley, M.J., Tipping, R.M., Clapperton, C.M., 2005. Evidence for late-glacial ice dammed lakes in the central strait of magellan and bahía inútil, southernmost South America. Geogr. Ann. Phys. Geogr. 87 (2), 335–362. https://doi.org/10.1111/j.0435-3676.2005.00262.x.

McCulloch, R.D., Bentley, M.J., Fabel, D., Fernández-Navarro, H., García, J.L., Hein, A.S., Huynh, C., Jamieson, S.S., Lira, M.P., Lüthgens, C., Nield, G.A., 2024. Resolving the paradox of conflicting glacial chronologies: reconstructing the pattern of deglaciation of the Magellan cordilleran ice dome (53–54° S) during the last glacial–interglacial transition. Quat. Sci. Rev., 108866

Mackay, H., Hughes, P.D., Jensen, B.J., Langdon, P.G., Pyne-O'Donnell, S.D., Plunkett, G., Froese, D.G., Coulter, S., Gardner, J.E., 2016. A mid to late Holocene cryptotephra framework from eastern North America. Quat. Sci. Rev. 132, 101–113.

Monteath, A.J., Hughes, P.D.M., Wastegård, S., 2019. Evidence for distal transport of reworked Andean tephra: extending the cryptotephra framework from the Austral volcanic zone. Quat. Geochronol. 51, 64–71. https://doi.org/10.1016/j.quageo.2019.01.003.

Monteath, A., Hughes, P., Cooper, M., Groff, D., Scaife, R., Hodgson, D., 2022. Late glacial–Holocene Record of Southern Hemisphere Westerly Wind Dynamics from the Falkland Islands, South Atlantic Ocean. Geology.

Moreno, P.I., Kaplan, M.R., François, J.P., Villa-Martínez, R., Moy, C.M., Stern, C.R., Kubik, P.W., 2009. Renewed glacial activity during the Antarctic cold reversal and persistence of cold conditions until 11.5 ka in southwestern Patagonia. Geology 37 (4), 375–378. https://doi.org/10.1130/G25399A.1.

Naranjo, J.A., Stern, C.R., 1998. Holocene explosive activity of Hudson volcano, Southern Andes. Bull. Volcanol. 59, 291–306. https://doi.org/10.1007/s004450050193.

Oppedal, L.T., van der Bilt, W.G., Balascio, N.L., Bakke, J., 2018. Patagonian ash on sub-Antarctic south Georgia: expanding the tephrostratigraphy of southern South America into the Atlantic sector of the Southern Ocean. J. Quat. Sci. 33 (5), 482–486. https://doi.org/10.1002/jqs.3035.

Panaretos, P., Albert, P.G., Thomas, Z.A., Turney, C.S., Stern, C.R., Jones, G., Williams, A. N., Smith, V.C., Hogg, A.G., Manning, C.J., 2021. Distal ash fall from the mid-holocene eruption of Mount Hudson (H2) discovered in the Falkland Islands: new possibilities for southern hemisphere archive synchronisation. Quat. Sci. Rev. 266, 107074 https://doi.org/10.1016/j.quascirev.2021.107074.

Payne, R.J., Kilfeather, A.A., van der Meer, J.J., Blackford, J.J., 2005. Experiments on the taphonomy of tephra in peat. Suo 147–156.

Payne, R., Gehrels, M., 2010. The formation of tephra layers in peatlands: an experimental approach. Catena 81 (1), 12–23.

Pedro, J.B., Bostock, H.C., Bitz, C.M., He, F., Vandergoes, M.J., Steig, E.J., Chase, B.M., Krause, C.E., Rasmussen, S.O., Markle, B.R., Cortese, G., 2016. The spatial extent and dynamics of the Antarctic cold reversal. Nat. Geosci. 9 (1), 51–55. https://doi.org/10.1038/ngeo2580.

Peccerillo, A., Taylor, S.R., 1976. Geochemistry of Eocene calc-alkaline volcanic rocks from the Kastamonu area, northern Turkey. Contrib. Mineral. Petrol. 58, 63–81.

Pilcher, J.R., Hall, V.A., 1992. Towards a tephrochronology for the Holocene of the north of Ireland. Holocene 2, 255–259.

Pizer, C.O., Howarth, J.D., Clark, K.J., Wilson, C.J., Tickle, S.E., Hopkins, J.L., Dahl, J.A., 2023. An integrated proximal-distal radiocarbon dating approach provides improved age constraints for a key Holocene tephra isochron. Quat. Sci. Rev. 307, 108069.

Scaife, R.G., Long, A.J., Monteath, A.J., Hughes, P.D., Bentley, M.J., Stone, P., 2019. The Falkland islands' palaeoecological response to millennial-scale climate perturbations during the Pleistocene–Holocene transition: implications for future vegetation stability in the southern ocean islands. J. Quat. Sci. 34 (8), 609–620.

Smith, R.E., Smith, V.C., Fontijn, K., Gebhardt, A.C., Wastegård, S., Zolitschka, B., Ohlendorf, C., Stern, C., Mayr, C., 2019. Refining the late Quaternary tephrochronology for southern South America using the Laguna Potrok Aike

sedimentary record. Quat. Sci. Rev. 218, 137–156. https://doi.org/10.1016/j.quascirev.2019.06.001.
Stern, C.R., 2004. Active Andean volcanism: its geologic and tectonic setting. Rev. Geol. Chile 31 (2), 1–51. https://doi.org/10.4067/S0716-02082004000200001.
Stern, C.R., 2008. Holocene tephrochronology record of large explosive eruptions in the southernmost Patagonian Andes. Bull. Volcanol. 70, 435–454. https://doi.org/10.1007/s00445-007-0148-z.
Stern, C.R., Moreno, P.I., Villa-Martinez, R., Sagredo, E.A., Prieto, A., Labarca, R., 2011. Evolution of ice-dammed proglacial lakes in Última Esperanza, Chile: implications from the late-glacial R1 eruption of Reclús volcano, Andean Austral Volcanic zone. Andean Geol. 38, 82–97.
Tamhane, J., Thomas, Z.A., Cadd, H., Harris, M.R., Turney, C., Marjo, C.E., Wang, H., Akter, R., Panaretos, P., Halim, A., Gadd, P.S., 2023. Mid-Holocene intensification of southern hemisphere westerly winds and implications for regional climate dynamics. Quat. Sci. Rev. 305, 108007 https://doi.org/10.1016/j.quascirev.2023.108007.
Tomlinson, E.L., Thordarson, T., Müller, W., Thirlwall, M., Menzies, M.A., 2010. Microanalysis of tephra by LA-ICP-MS—strategies, advantages and limitations assessed using the Thorsmörk Ignimbrite (southern Iceland). Chem. Geol. 279 (3–4), 73–89. https://doi.org/10.1016/j.chemgeo.2010.09.013.
Thomas, Z.A., Jones, R.T., Fogwill, C.J., Hatton, J., Williams, A.N., Hogg, A., Mooney, S., Jones, P., Lister, D., Mayewski, P., Turney, C.S.M., 2018. Evidence for increased expression of the Amundsen Sea low over the south Atlantic during the late Holocene. Clim. Past 14 (11), 1727–1738. https://doi.org/10.5194/cp-14-1727-2018.
Thomas, Z.A., Turney, C.S.M., Hogg, A.G., Williams, A.N., Fogwill, C.J., 2019. Investigating subantarctic ^{14}C ages of different peat components: site and sample selection for developing robust age models in dynamic landscapes. Radiocarbon 61 (4), 1009–1027. https://doi.org/10.1017/RDC.2019.54.
Turney, C.S.M., Jones, R.T., Fogwill, C., Hatton, J., Williams, A.N., Hogg, A., Thomas, Z. A., Palmer, J., Mooney, S., Reimer, R.W., 2016. A 250-year periodicity in southern hemisphere westerly winds over the last 2600 years. Clim. Past 12, 189–200. https://doi.org/10.5194/cp-12-189-2016.
Turney, et al., 2021. Radiocarbon Protocols and First Intercomparison Results from the Chronos ^{14}Carbon-Cycle Facility. University of New South Wales, Sydney, Australia. Radiocarbon.
Upton, J., Shaw, C.J., 2002. An overview of the oceanography and meteorology of the Falkland Islands. Aquat. Conserv. Mar. Freshw. Ecosyst. 12, 15–25. https://doi.org/10.1002/aqc.496.
Van Daele, M., Bertrand, S., Meyer, I., Moernaut, J., Vandoorne, W., Siani, G., Tanghe, N., Ghazoui, Z., Pino, M., Urrutia, R., De Batist, M., 2016. Late Quaternary evolution of Lago Castor (Chile, 45.6?S): timing of the deglaciation in northern Patagonia and evolution of the southern westerlies during the last 17 kyr. Quat. Sci. Rev. 133, 130e146. https://doi.org/10.1016/j.quascirev.2015.12.021.
Villa-Martínez, R., Moreno, P.I., 2007. Pollen evidence for variations in the southern margin of the westerly winds in SW Patagonia over the last 12,600 years. Quaternary Research 68 (3), 400–409. https://doi.org/10.1016/j.yqres.2007.07.003.
Watson, E.J., Swindles, G.T., Lawson, I.T., Savov, I.P., 2015. Spatial variability of tephra and carbon accumulation in a Holocene peatland. Quat. Sci. Rev. 124, 248–264.
Watt, S.F., Pyle, D.M., Mather, T.A., 2013. Evidence of mid-to late-holocene explosive rhyolitic eruptions from Chaitén Volcano, Chile. Andean Geol. 40 (2), 216–226.
Wastegård, S., Veres, D., Kliem, P., Hahn, a., Ohlendorf, C., Zolitschka, B., 2013. Towards a late Quaternary tephrochronological framework for the southernmost part of South America - the Laguna Potrok Aike tephra record. Quat. Sci. Rev. 71, 81–90. https://doi.org/10.1016/j.quascirev.2012.10.019.
Weller, D.J., Miranda, C.G., Moreno, P.I., Villa-Martínez, R., Stern, C.R., 2015. Tephrochronology of the southernmost Andean southern volcanic zone, Chile. Bull. Volcanol. 77, 1–24. https://doi.org/10.1007/s00445-015-0991-2.
Weller, D.J., Porras, M. E. De, Maldonado, A., Mendez, C., Stern, C.R., 2018. New age controls on the tephrochronology of the southernmost Andean southern vol- canic zone, Chile. Quat. Res. 91 (1), 1–5. https://doi.org/10.1017/qua.2018.81.
Wilson, P., Clark, R., Birnie, J., Moore, D.M., 2002. Late Pleistocene and Holocene landscape evolution and environmental change in the Lake Sulivan area, Falkland Islands, South Atlantic. Quat. Sci. Rev. 21, 1821–1840.
Zanchetta, G., Pappalardo, M., Di Roberto, A., Bini, M., Arienzo, I., Isola, I., Boretto, G., Fuck, E., Mele, D., D'Orazio, M., Passariello, I., 2021. A Holocene tephra layer within coastal aeolian deposits north of Caleta Olivia (Santa Cruz Province, Argentina). Andean Geol. 48 (2), 267–280. https://doi.org/10.5027/andgeoV48n2-3290.